ACADEMIC PRESS

Available online at www.sciencedirect.com

SCIENCE DIRECT®

Journal of Computational Physics 184 (2003) 619–648

JOURNAL OF COMPUTATIONAL PHYSICS

www.elsevier.com/locate/jcp

Variational mesh adaptation II: error estimates and monitor functions

Weizhang Huang [a,*,1], Weiwei Sun [b,2]

[a] *Department of Mathematics, The University of Kansas, Lawrence, KS 66045, USA*
[b] *Department of Mathematics, City University of Hong Kong, Kowloon, Hong Kong, PR China*

Received 10 December 2001; received in revised form 8 October 2002; accepted 18 October 2002

Abstract

The key to the success of a variational mesh adaptation method is to define a proper monitor function which controls mesh adaptation. In this paper we study the choice of the monitor function for the variational adaptive mesh method developed in the previous work [J. Comput. Phys. 174 (2001) 924]. Two types of monitor functions, scalar matrix and non-scalar matrix ones, are defined based on asymptotic estimates of interpolation error obtained using the interpolation theory of finite element methods. The choice of the adaptation intensity parameter is also discussed for each of these monitor functions. Asymptotic bounds on interpolation error are obtained for adaptive meshes that satisfy the regularity and equidistribution conditions. Two-dimensional numerical results are given to verify the theoretical findings.

Keywords: Mesh adaptation; Coordinate transformation; Variational method; Error estimate; Monitor function

1. Introduction

In this paper we are concerned with variational mesh adaptation in the numerical solution of partial differential equations. A variational method utilizes a functional to determine the coordinate transformation needed for mesh generation. Such a functional is often formulated to measure difficulties in the numerical approximation of the physical solution, and typically involves a so-called monitor function that is prescribed by the user to control mesh concentration.

The most straightforward approach of formulating an adaptation functional is to directly minimize a certain error or one of its bounds. Unfortunately, this approach often leads to an ill-conditioned

* Corresponding author. Tel.: 1-785-864-3651; fax: 1-785-864-5255.
E-mail addresses: huang@math.ukans.edu (W. Huang), maweiw@math.cityu.edu.hk (W. Sun).
[1] This author was supported in part by the NSF (USA) through Grant DMS–0074240.
[2] This author was supported in part by a grant from the Research Grants Council of the Hong Kong Special Administrative Region, China (Project No. CityU 1084/02P) and City University of Hong Kong Research Grant 7001331.

0021-9991/02/$ - see front matter
PII: S0021-9991(02)00040-2

minimization problem and thus has rarely been used in the past. Instead, almost all of the existing variational methods have been developed based on geometric considerations; e.g., see [5,6,11,14,17,19,20,25,29] and the books [12,18,22,26] and references therein. For example, Brackbill and Saltzman [6] develop a popular method by combining mesh concentration, smoothness, and orthogonality. Dvinsky [11] uses the energy of harmonic mappings as his mesh adaptation functional. Knupp [17,19] and Knupp and Robidoux [20] develop functionals based on the idea of conditioning the Jacobian matrix of the coordinate transformation. But, these geometry-based variational methods are not without problems. Their lacking a direct connection with some error makes it tricky to choose a proper monitor function for practical problems. It also makes it extremely difficult to perform error analysis on the resulting adaptive meshes.

Motivated by the need of an error-oriented as well as well-conditioned mesh adaptation functional, Huang [16] has recently proposed a new method based on the isotropy (or regularity) and equidistribution criteria. These criteria are devised from the requirement that the physical solution be well resolved in the computational domain by a uniform mesh. The developed mesh adaptation functional leads to a reasonably well-conditioned mesh system and is directly connected to interpolation error of a function.

In this paper we continue the development of [16] and investigate the in-depth relation of the new method with interpolation error. The key to the success of a variational mesh adaptation method is to choose a proper monitor function which controls mesh adaptation. The objective of this work is to define the monitor function for the new variational method based on estimates of interpolation error. To this end, we first develop several asymptotic estimates for interpolation error in terms of a coordinate transformation between the physical and computational domains. The main tool we use is the interpolation theory of finite element methods. We then carry the estimation further using the so-called regularity and equidistribution condition: see (41) and (42). (To some extent, minimizing the functional of [16] tends to minimize the functions on the left-hand sides of the conditions.) The monitor function and bounds on interpolation error are finally obtained.

An outline of this paper is as follows. In Section 2 we briefly describe the variational mesh adaptation method of [16]. In Section 3 interpolation error estimates are developed in terms of a coordinate transformation between the physical and computational domains. These results are used in Section 4 to define both scalar (Winslow's type) and non-scalar matrix monitor functions. (A scalar matrix is defined as the product of a scalar function with the identity matrix.) In the same section, the choice of the intensity parameter is discussed, and error bounds on adaptive meshes are obtained under the regularity and equidistribution conditions that formulate the approximate satisfaction of the isotropy and equidistribution criteria. Two-dimensional numerical results are presented in Section 5 to show that the method of [16], together with the monitor functions developed in Section 4, is able to produce adaptive meshes that satisfy the conditions. Finally, conclusions are drawn in Section 6.

2. Variational mesh adaptation

Denote by $\Omega \subset \mathbb{R}^n$, $n = 1, 2$, or 3 the physical domain and Ω_c the logical or computational domain which is chosen artificially for the purpose of mesh adaptation. We consider mesh generation as a mathematical equivalent of determining a one-to-one coordinate transformation $\boldsymbol{x} = \boldsymbol{x}(\boldsymbol{\xi})$ from Ω_c to Ω in the sense that adaptive meshes are generated as images of a prescribed and often uniform computational mesh under $\boldsymbol{x} = \boldsymbol{x}(\boldsymbol{\xi})$. The coordinate transformation is defined in a variational method as the minimizer of a functional measuring difficulties in the numerical approximation of the physical solution.

A new strategy of formulating the adaptation functional is proposed in [16]. That is, the coordinate transformation is sought such that, for a given $n \times n$ symmetric positive definite matrix $G = G(\boldsymbol{x})$ (which is often referred to as the monitor function), the "error" function

$$E(\boldsymbol{\xi}) = \sqrt{(\boldsymbol{\xi}-\boldsymbol{\xi}_0)^{\mathrm{T}}\boldsymbol{J}(\boldsymbol{\xi}_0)^{\mathrm{T}}G(x(\boldsymbol{\xi}_0))\boldsymbol{J}(\boldsymbol{\xi}_0)(\boldsymbol{\xi}-\boldsymbol{\xi}_0)} \tag{1}$$

is uniformly distributed about $\boldsymbol{\xi}_0 \in \Omega_c$. This requires

$$\boldsymbol{J}^{-1}G^{-1}\boldsymbol{J}^{-\mathrm{T}} = cI, \tag{2}$$

where $\boldsymbol{J} = (\partial \boldsymbol{x})/(\partial \boldsymbol{\xi})$, for some positive constant c. Criterion (2) is equivalent to the combination of the following conditions:

Isotropy criterion:

$$\lambda_1 = \cdots = \lambda_n, \tag{3}$$

Equidistribution criterion:

$$\sqrt{\prod_i \lambda_i} = \text{constant}, \tag{4}$$

where $\lambda_i, i = 1, \ldots, n$, are the eigenvalues of $\boldsymbol{J}^{-1}G^{-1}\boldsymbol{J}^{-\mathrm{T}}$.

Regarding the isotropy criterion, the refined version of the arithmetic–geometric mean inequality [21] leads to

$$\frac{1}{n(n-1)}\sum_{i<j}\left(\sqrt{\lambda_i}-\sqrt{\lambda_j}\right)^2 \leqslant \frac{1}{n}\sum_i \lambda_i - \left(\prod_i \lambda_i\right)^{\frac{1}{n}} \leqslant \frac{1}{n}\sum_{i<j}\left(\sqrt{\lambda_i}-\sqrt{\lambda_j}\right)^2. \tag{5}$$

For some number $q \geqslant 1$, Jensen's inequality gives

$$\left(\frac{1}{n}\sum_i \lambda_i\right)^{\frac{nq}{2}} - \left(\prod_i \lambda_i\right)^{\frac{q}{2}} \geqslant \left[\frac{1}{n(n-1)}\sum_{i<j}(\sqrt{\lambda_i}-\sqrt{\lambda_j})^2\right]^{\frac{nq}{2}}. \tag{6}$$

This shows that λ_i's can be made to be as equal as possible by minimizing the left-hand side of the inequality. Notice that

$$\sum_i \lambda_i = \mathrm{tr}(\boldsymbol{J}^{-1}G^{-1}\boldsymbol{J}^{-\mathrm{T}}) = \sum_i (\nabla \xi^i)^{\mathrm{T}} G^{-1} \nabla \xi^i, \quad \prod_i \lambda_i = \det(\boldsymbol{J}^{-1}G^{-1}\boldsymbol{J}^{-\mathrm{T}}) = \frac{1}{J^2 g},$$

where J and g are the determinants of $\boldsymbol{J}$ and G, respectively. Multiplying the left-hand side of (6) with $\sqrt{g}$ and integrating over Ω, we obtain the isotropy functional

$$I_{\mathrm{iso}}[\boldsymbol{\xi}] = \int_\Omega \left[\sqrt{g}\left(\sum_i (\nabla \xi^i)^{\mathrm{T}} G^{-1} \nabla \xi^i\right)^{\frac{nq}{2}} - n^{\frac{nq}{2}} \frac{\sqrt{g}}{(J\sqrt{g})^q}\right] \mathrm{d}\boldsymbol{x}. \tag{7}$$

On the other hand, the equidistribution criterion (4) can be rewritten as

$$J\sqrt{g} = \sigma, \tag{8}$$

where σ is a constant that can be found from (8), viz.,

$$\sigma = \frac{1}{|\Omega_c|}\int_\Omega \sqrt{g}\,\mathrm{d}\boldsymbol{x}. \tag{9}$$

Eq. (8) is a multi-dimensional generalization of the well-known (one-dimensional) equidistribution principle [10]. Function $J\sqrt{g}$ can be made to be as flat as possible by minimizing the functional

$$I_{\mathrm{ep}}[\boldsymbol{\xi}] = \int_{\Omega} \frac{\sqrt{g}}{(J\sqrt{g})^q}\,\mathrm{d}\boldsymbol{x} \tag{10}$$

for some $q > 1$.

A functional balancing isotropy and equidistribution is obtained in [16] by combining $I_{\mathrm{iso}}[\boldsymbol{\xi}]$ and $I_{\mathrm{ep}}[\boldsymbol{\xi}]$, i.e.,

$$I[\boldsymbol{\xi}] = \theta \int_{\Omega} \sqrt{g}\left(\sum_i (\nabla\xi^i)^{\mathrm{T}} G^{-1} \nabla\xi^i\right)^{\frac{nq}{2}} \mathrm{d}\boldsymbol{x} + (1-2\theta)n^{\frac{nq}{2}} \int_{\Omega} \frac{\sqrt{g}}{(J\sqrt{g})^q}\,\mathrm{d}x, \tag{11}$$

where $\theta \in (0, 1/2]$ and $q \geqslant 1$. Note that the integrals in (11) have the same dimension and thus the weight parameter θ is dimensionless. The smaller θ is, the closer the equidistribution (8) is satisfied. Moreover, the second integral becomes constant for $q = 1$ and vanishes for $\theta = 1/2$. In these situations, $I[\boldsymbol{\xi}]$ is equivalent or equal to the first integral, which is a well-conditioned functional in the sense that its minimizer exists uniquely and satisfies the maximum principle: e.g., see [13,23]. A special case is $q = 1$ and $n = 2$, where $I[\boldsymbol{\xi}]$ becomes the energy functional of harmonic mappings. It is known [11,24] that a two-dimensional harmonic mapping is non-singular if Ω_c is convex.

$I[\boldsymbol{\xi}]$ appears to have minimizers. This is because $I[\boldsymbol{\xi}]$ is coercive for $\theta \in (0, 1/2]$ and the non-convexity part of the functional – the equidistribution integral – is known (at least numerically) to have many minimizers. A minimizer of $I[\boldsymbol{\xi}]$ seems to be non-singular too. When θ is close 1/2, the second integral can be considered as a perturbation to the first one. Thus, the minimizer of $I[\boldsymbol{\xi}]$ is close to the unique and non-singular minimizer of the first integral and therefore is non-singular. On the other hand, when θ is close to zero, the second part of (11) dominates the functional and the equidistribution (8) is satisfied closely. As a consequence, a minimizer satisfying (8) is locally non-singular.

For $q > 1$, the first integral in (11) is not quadratic. Nevertheless, the numerical solution for its minimizer is relatively easy because of its convexity. The main difficulty comes from the equidistribution part. Indeed, we do experience convergence difficulties in non-linear iteration for small values of θ (e.g. $\theta = 0.001$) for very rough physical solutions. In this situation, we recommend to use under-relaxation in the non-linear iteration. A continuation procedure in θ will also be helpful.

3. Interpolation error estimates

In this section we develop interpolation error estimates in terms of coordinate transformations between Ω and Ω_c. The results will be used in Section 4 for defining the monitor function $G = G(\boldsymbol{x})$, the key to the success of the variational mesh adaptation method described in the preceding section.

3.1. The classic results

Let $\hat{D}$ and $D = F(\hat{D})$ be affine equivalent open subsets of $\mathbb{R}^n$, where F is an invertible affine mapping. Denote by $\|\cdot\|$ and $\|\cdot\|_F$ the Euclidean and Frobenius matrix norms, respectively. Let C be the generic constant. For notational simplicity, we assume in this section that, when appearing simultaneously in one equation, function v defined in D and function $\hat{v}$ defined in $\hat{D}$ are related to each other through $v = \hat{v} \circ F^{-1}$ or $\hat{v} = v \circ F$.

The results of the following three lemmas are standard in the context of finite element methods. The interested reader is referred to [9] for their proofs.

Lemma 3.1. *For $m \geqslant 0$, there exists a constant $C = C(m,n)$ such that*

$$|\hat{v}|_{m,\hat{D}} \leqslant C\|F'\|^m \cdot |\det(F')|^{-\frac{1}{2}} \cdot |v|_{m,D} \quad \forall v \in H^m(D),$$

where F' is the Jacobian matrix of mapping F and $|\cdot|_{m,\hat{D}}$ and $|\cdot|_{m,D}$ denote the semi-norms of Sobolev spaces $H^m(\hat{D})$ and $H^m(D)$, respectively. Similarly,

$$|v|_{m,D} \leqslant C\|(F')^{-1}\|^m \cdot |\det(F')|^{\frac{1}{2}} \cdot |\hat{v}|_{m,\hat{D}} \quad \forall \hat{v} \in H^m(\hat{D}).$$

Lemma 3.2. *Denote by h_D the diameter and ρ_D the in-diameter of D, i.e., $h_D = \operatorname{diam}(D)$ and $\rho_D = \sup\{\operatorname{diam}(S) : S \text{ is a ball contained in } D\}$. Define $h_{\hat{D}}$ and $\rho_{\hat{D}}$ similarly. Then,*

$$\|F'\| \leqslant \frac{h_D}{\rho_{\hat{D}}} \quad \text{and} \quad \|(F')^{-1}\| \leqslant \frac{h_{\hat{D}}}{\rho_D}.$$

Lemma 3.3. *For some integers m and k: $0 \leqslant m \leqslant k+1$, let $H^m(\hat{D})$ and $H^{k+1}(\hat{D})$ be Sobolev spaces and let $\hat{\Pi} \in \mathscr{L}(H^{k+1}(\hat{D}); H^m(\hat{D}))$ be an operator such that*

$$\hat{\Pi}\hat{p} = \hat{p} \quad \forall \hat{p} \in P_k(\hat{D}),$$

where $P_k(\hat{D})$ is the space of polynomials of degree no more than k. Then,

$$|\hat{v} - \hat{\Pi}\hat{v}|_{m,\hat{D}} \leqslant C(\hat{\Pi}, \hat{D}) \cdot |\hat{v}|_{k+1,\hat{\Omega}} \quad \forall \hat{v} \in H^{k+1}(\hat{D}).$$

The classic estimate for interpolation error can readily be obtained from the above lemmas. Indeed, assume that $\{T_h\}$ is a regular family of quasi-uniform triangulations in Ω, viz.,

Regularity:

$$h \equiv \max_{K \in T_h} h_K \to 0, \quad \max_{T_h \in \{T_h\}} \max_{K \in T_h} \frac{h_K}{\rho_K} \leqslant C_1. \tag{12}$$

Quasi-uniformity:

$$\frac{\max\limits_{K \in T_h} h_K}{\min\limits_{K \in T_h} h_K} \leqslant C_2 \quad \forall T_h \in \{T_h\}. \tag{13}$$

For each $K \in T_h$, define $\Pi \in \mathscr{L}(H^{k+1}(K); H^m(K))$ as

$$\Pi w = (\hat{\Pi}(w \circ F)) \circ F^{-1} \quad \forall w \in H^{k+1}(K),$$

where $\hat{\Pi}$ is the interpolation operator defined in the master element $\hat{K}$. It follows from Lemma 3.3 that

$$\sum_{K \in T_h} |v - \Pi v|^2_{m,K} \leqslant Ch^{2(k+1-m)}|v|^2_{k+1} \quad \forall v \in H^{k+1}(\Omega), \quad 0 \leqslant m \leqslant k. \tag{14}$$

3.2. Local error estimates

We now begin error estimation with defining the coordinate transformation. Assume that an affine family $\{T_h\}$ of triangulations in Ω are given so that there exists an invertible affine mapping F between the

master element $\hat{K}$ and each element $K \in T_h$. We also assume that the computational domain Ω_c and the family $\{T_{h_c}\}$ of its triangulations are chosen such that

(i) For any triangulation T_h on Ω, there exists a unique triangulation $T_{h_c} \in \{T_{h_c}\}$ having the same connectivity and the same number of elements of T_h.
(ii) The family $\{T_{h_c}\}$ of triangulations in the computational domain is affine, regular, and quasi-uniform.

Note that we have not made any assumption on the regularity (such as quasi-uniformity) of the physical triangulations. Indeed, avoiding such a restriction is generally necessary for meaningful analysis of mesh adaptation. On the other hand, the regularity assumptions for $\{T_{h_c}\}$ are necessary for the convergence of the polynomial approximation as the mesh is refined.

For an arbitrary element $K_c \in T_{h_c}$, let G be the invertible affine mapping between $\hat{K}$ and K_c. From Lemma 3.2 and the fact that $h_{\hat{K}} = \mathrm{O}(1)$ and $\rho_{\hat{K}} = \mathrm{O}(1)$ for the master element $\hat{K}$, the assumption (ii) implies

$$\|G'\| \leqslant Ch_c \quad \text{and} \quad \|(G')^{-1}\| \leqslant \frac{C}{h_c} \quad \forall K_c \in T_{h_c}. \tag{15}$$

Assumption (i) warrants the existence of a one-to-one correspondence between the elements of T_h and their counterparts in T_{h_c}. Given an element $K \in T_h$, denote by K_c the corresponding element in T_{h_c}. The restriction of $\boldsymbol{\xi} = \boldsymbol{\xi}(\boldsymbol{x}) : \Omega \to \Omega_c$ on K can be defined as

$$\boldsymbol{\xi}|_K = G \circ F^{-1}. \tag{16}$$

The relations among $\hat{K}$, K and K_c are illustrated in Fig. 1. (Note that the elements we consider are not necessarily triangles as illustrated in the figure.)

Theorem 3.1. *For given integers m and $k : 0 \leqslant m \leqslant k+1$, let $H^{k+1}(\hat{K})$ and $H^m(\hat{K})$ be two Sobolev spaces and let $\hat{\Pi} \in \mathscr{L}(H^{k+1}(\hat{K}); H^m(\hat{K}))$ be an operator such that*

$$\hat{\Pi}\hat{p} = \hat{p} \quad \forall \hat{p} \in P_k(\hat{K}).$$

Then

$$|v - \Pi v|_{m,K} \leqslant Ch_c^{k+1-m} \|\boldsymbol{J}^{-1}\|^m \|\boldsymbol{J}\|^{k+1} \cdot |v|_{k+1,K} \quad \forall v \in H^{k+1}(K), \tag{17}$$

$$|v - \Pi v|_{m,K} \leqslant Ch_c^{k+1-m} J^{-\frac{1}{2}} \|\boldsymbol{J}^{-1}\|^m \cdot |v \circ \boldsymbol{\xi}^{-1}|_{k+1,K_c} \quad \forall v \in H^{k+1}(K). \tag{18}$$

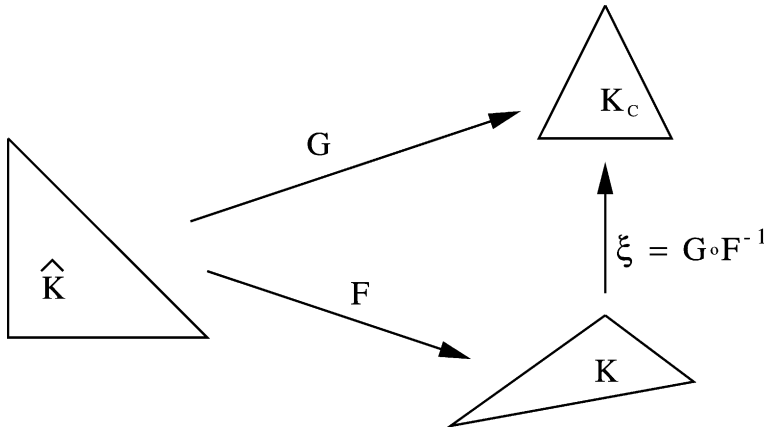

Fig. 1. The relations among the physical (K), computational (K_c), and master ($\hat{K}$) elements.

Proof. From $F = \boldsymbol{\xi}^{-1} \circ G$ and $F^{-1} = G^{-1} \circ \boldsymbol{\xi}$, (15) implies that

$$\|F'\| \leqslant Ch_c \|\boldsymbol{J}\|, \quad \|(F')^{-1}\| \leqslant Ch_c^{-1} \|\boldsymbol{J}^{-1}\|. \tag{19}$$

Taking $D = K$ and $\hat{D} = \hat{K}$ in Lemmas 3.1 and 3.3, we get

$$|v - \Pi v|_{m,K} \leqslant C\|(F')^{-1}\|^m \cdot |\det(F')|^{\frac{1}{2}} \cdot |\hat{v}|_{k+1,\hat{K}}. \tag{20}$$

Combining (20) with Lemma 3.1 and (19) leads to (17).

On the other hand, taking $D = K_c$ and $\hat{D} = \hat{K}$ in Lemma 3.1 we get

$$|\hat{v}|_{k+1,\hat{K}} \leqslant C\|G'\|^{k+1} |\det(G')|^{-\frac{1}{2}} |\hat{v} \circ G^{-1}|_{k+1,K_c}. \tag{21}$$

Combining (20) with (21) results in

$$|v - \Pi v|_{m,K} \leqslant C\|(F')^{-1}\|^m |\det(F')|^{\frac{1}{2}} \|G'\|^{k+1} |\det(G')|^{-\frac{1}{2}} |\hat{v} \circ G^{-1}|_{k+1,K_c}. \tag{22}$$

Estimate (18) follows from (19), (22), $\det(F') = \det(\boldsymbol{J}) \det(G')$, and the fact that $\hat{v} \circ G^{-1} = v \circ F \circ G^{-1} = v \circ \boldsymbol{\xi}^{-1}$. □

Remark 3.1. For simplicity, we confine ourselves in this paper to functions with the optimal regularity for kth degree polynomial preserving operators, i.e., functions of $H^{k+1}(K)$. However, it is worth pointing out that the strategy used here will also work for functions with lower regularity, e.g., those of $H^l(K)$ with $1 \leqslant l \leqslant k+1$, although the convergence order of interpolation error will be reduced accordingly.

3.3. Global error estimates

We now proceed with global error estimation. For an arbitrary matrix A, it is not difficult to show

$$\|A\| \leqslant \|A\|_F, \quad \|A\|_F^2 = \operatorname{tr}(A^{\mathrm{T}}A), \quad \|A^{-1}\|_F^2 = \left\| \frac{\operatorname{Adj}(A)}{\det(A)} \right\|_F^2 \leqslant \frac{C}{\det(A)^2} \|A\|_F^{2(n-1)}. \tag{23}$$

Recalling that the mapping $\boldsymbol{\xi} = \boldsymbol{\xi}(\boldsymbol{x})$ is piecewise linear and the Jacobian matrix $\boldsymbol{J}$ is constant in each element, from (17) we have

$$\begin{aligned}
\sum_K |v - \Pi v|_{m,K}^2 &\leqslant Ch_c^{2(k+1-m)} \sum_K \|\boldsymbol{J}^{-1}\|_F^{2m} \cdot \|\boldsymbol{J}\|_F^{2(k+1)} \cdot \int_K \|\partial^{k+1} v\|_F^2 \, \mathrm{d}\boldsymbol{x} \\
&\leqslant Ch_c^{2(k+1-m)} \sum_K \int_K \|\boldsymbol{J}^{-1}\|_F^{2m} \cdot \|\boldsymbol{J}\|_F^{2(k+1)} \cdot \|\partial^{k+1} v\|_F^2 \, \mathrm{d}\boldsymbol{x} \\
&\leqslant Ch_c^{2(k+1-m)} \sum_K \int_K \frac{1}{J^{2m}} \cdot \|\boldsymbol{J}\|_F^{2(k+1)+2m(n-1)} \cdot \|\partial^{k+1} v\|_F^2 \, \mathrm{d}\boldsymbol{x},
\end{aligned}$$

where ∂ is the differential operator with respect to $\boldsymbol{x}$. Thus,

$$\sum_K |v - \Pi v|_{m,K}^2 \leqslant Ch_c^{2(k+1-m)} \sum_K \int_k \frac{1}{J^{2m}} \cdot \left[\operatorname{tr}(\boldsymbol{J}^{\mathrm{T}}\boldsymbol{J})\right]^{k+1+m(n-1)} \cdot \|\partial^{k+1} v\|_F^2 \, \mathrm{d}\boldsymbol{x}. \tag{24}$$

Similarly, from (18) and (23) we get

$$\sum_K |v - \Pi v|_{m,K}^2 \leqslant Ch_c^{2(k+1-m)} \sum_K \int_k \frac{1}{J^{2m}} \cdot \left[\operatorname{tr}(\boldsymbol{J}^{\mathrm{T}}\boldsymbol{J})\right]^{m(n-1)} \cdot \|\partial_{\boldsymbol{\xi}}^{k+1} v\|_F^2 \, \mathrm{d}\boldsymbol{x}, \tag{25}$$

where ∂_ξ denotes the differential operator with respect to $\boldsymbol{\xi}$. Since $\partial_\xi^{k+1} v$ has a very complicated expression in terms of derivatives with respect to $\boldsymbol{x}$ for large k, we consider here two simple but widely used cases, piecewise constant interpolation ($k = 0$) and piecewise linear interpolation ($k = 1$).

For the case ($k = 0$), the chain-rule gives

$$\frac{\partial v}{\partial \xi^i} = \sum_j \frac{\partial v}{\partial x_j}\frac{\partial x_j}{\partial \xi^i} = (\nabla v)^{\mathrm{T}} \boldsymbol{a}_i,$$

where $\boldsymbol{a}_i = (\partial \boldsymbol{x})/(\partial \xi^i)$ is a convariant base vector. Thus,

$$\|\nabla_\xi v\|_F^2 = \sum_i \boldsymbol{a}_i^{\mathrm{T}} \nabla v (\nabla v)^{\mathrm{T}} \boldsymbol{a}_i = \mathrm{tr}(\boldsymbol{J}^{\mathrm{T}} \nabla v (\nabla v)^{\mathrm{T}} \boldsymbol{J}).$$

Substituting this into (25) yields

$$\sum_K \|v - \Pi v\|_K^2 \leqslant C h_c^2 \sum_K \int_K \mathrm{tr}(\boldsymbol{J}^{\mathrm{T}} \nabla v (\nabla v)^{\mathrm{T}} \boldsymbol{J})\,\mathrm{d}\boldsymbol{x}. \tag{26}$$

For the case $k = 1$, from the chain-rule and the fact that the mapping $\boldsymbol{\xi}(\boldsymbol{x})$ is piecewise linear, we have

$$\frac{\partial^2 v}{\partial \xi^\alpha \partial \xi^\beta} = \sum_{ij} \frac{\partial^2 v}{\partial x_i \partial x_j}\frac{\partial x_i \partial x_j}{\partial \xi^\alpha \partial \xi^\beta} = \boldsymbol{a}_\alpha^{\mathrm{T}} H \boldsymbol{a}_\beta, \quad \|\partial_\xi^2 v\|_F^2 = \sum_{ij} (\boldsymbol{a}_i^{\mathrm{T}} H \boldsymbol{a}_j)^2,$$

where $H = ((\partial^2 v)/(\partial x_i \partial x_j))$ is the Hessian matrix of v. Let the eigen-decomposition of H be

$$H = Q\,\mathrm{diag}(\mu_1, \ldots, \mu_n) Q^{\mathrm{T}}.$$

Define

$$|H| = Q\,\mathrm{diag}(|\mu_1|, \ldots, |\mu_n|) Q^{\mathrm{T}}.$$

It is easy to show

$$|\boldsymbol{a}_i^{\mathrm{T}} H \boldsymbol{a}_j| \leqslant \tfrac{1}{2}(\boldsymbol{a}_i^{\mathrm{T}} |H| \boldsymbol{a}_i + \boldsymbol{a}_j^{\mathrm{T}} |H| \boldsymbol{a}_j).$$

Thus,

$$\|\partial_\xi^2 v\|_F^2 \leqslant n \sum_i \left(\boldsymbol{a}_i^{\mathrm{T}} |H| \boldsymbol{a}_i\right)^2 \leqslant n \left(\sum_i \boldsymbol{a}_i^{\mathrm{T}} |H| \boldsymbol{a}_i\right)^2 = n\left[\mathrm{tr}(\boldsymbol{J}^{\mathrm{T}} |H| \boldsymbol{J})\right]^2. \tag{27}$$

From (25), we get

$$\sum_k |v - \Pi v|_{m,k}^2 \leqslant C h_c^{2(2-m)} \sum_K \int_K \frac{1}{J^{2m}} \cdot \left[\mathrm{tr}(\boldsymbol{J}^{\mathrm{T}} \boldsymbol{J})\right]^{m(n-1)} \cdot \left[\mathrm{tr}(\boldsymbol{J}^{\mathrm{T}} |H| \boldsymbol{J})\right]^2 \mathrm{d}\boldsymbol{x} \tag{28}$$

for $m = 0$ or $m = 1$.

The estimates (24), (26), and (28) have been obtained under the assumption that the mapping $\boldsymbol{\xi} = \boldsymbol{\xi}(\boldsymbol{x})$ is piecewise linear. On one hand, this is true for most computations with the variational mesh adaptation. On the other hand, we can hope that the estimates are asymptotically correct when the mapping is not piecewise linear. For these reasons and especially the latter one, we will ignore the piecewise linearity restriction and use the estimates for any smooth coordinate transformation on any type of meshes.

To summarize, we have from (24) that, for some integers $0 \leqslant m \leqslant k + 1$ and some kth polynomial preserving operator Π,

$$|v - \Pi v|_m^2 \lesssim C h_c^{2(k+1-m)} B_1[\xi] \quad \forall v \in H^{k+1}(\Omega), \tag{29}$$

where $\lesssim$ denotes "asymptotically less than or equal to" and

$$B_1[\xi] = \int_\Omega \frac{1}{J^{2m}} \left(\mathrm{tr}(J^{\mathrm{T}} J)\right)^{k+1+m(n-1)} \|\partial^{k+1} v\|_F^2 \, \mathrm{d}x. \tag{30}$$

For piecewise constant interpolation ($k = 0$), (26) gives

$$\|v - \Pi v\|^2 \lesssim C h_c^2 B_2[\xi] \quad \forall v \in H^1(\Omega), \tag{31}$$

where

$$B_2[\xi] = \int_\Omega \mathrm{tr}(J^{\mathrm{T}} \nabla v (\nabla v)^{\mathrm{T}} J) \, \mathrm{d}x. \tag{32}$$

For piecewise linear interpolation ($k = 1$), we have from (28) that, for $m = 0$ or $m = 1$,

$$|v - \Pi v|_m^2 \lesssim C h_c^{2(2-m)} B_3[\xi] \quad \forall v \in H^2(\Omega), \tag{33}$$

where

$$B_3[\xi] = \int_\Omega \frac{1}{J^{2m}} \cdot \left[\mathrm{tr}(J^{\mathrm{T}} J)\right]^{m(n-1)} \left[\mathrm{tr}(J^{\mathrm{T}} |H| J)\right]^2 \mathrm{d}x. \tag{34}$$

These error estimates may be used for mesh adaptation in various ways. The most straightforward approach is to directly minimize the functional B_1, B_2, or B_3. Unfortunately, there are several drawbacks associated with this approach. First of all, functionals B_1, B_2, and B_3 are non-convex and the existence of their minimizers is unknown. Moreover, it is unclear whether or not their minimizers, if any, are non-singular or at least satisfy some type of maximum principles. It is believed that the maximum principle provides a mechanism to prevent the mapping from becoming singular. Furthermore, B_1, B_2, and B_3 are highly non-linear, no matter whether they are viewed as functionals of $x(\xi)$ or $\xi(x)$. This can be seen more clearly from, e.g., the forms

$$B_2[x] = \int_{\Omega_c} \sum_i a_i^{\mathrm{T}} \nabla v (\nabla v)^{\mathrm{T}} a_i J \, \mathrm{d}\xi \tag{35}$$

with $J = a_1 \cdot (a_2 \times a_3)$ and

$$B_2[\xi] = \int_\Omega \sum_i \frac{1}{(1/J)^2} (a^j \times a^k)^{\mathrm{T}} \nabla v (\nabla v)^{\mathrm{T}} (a^j \times a^k) \, \mathrm{d}x \quad (i, j, k) \text{ cyclic}, \tag{36}$$

where $a^i = \nabla \xi^i$ is a contravariant base vector and the Jacobian has the relation $1/J = a^1 \cdot (a^2 \times a^3)$. The high degree of non-linearity makes it extremely difficult to find a minimizer numerically.

Due to these drawbacks, we will not use the direct minimization approach in this work. Instead, we consider the variational approach described in the preceding section that attempts to equidistribute rather than minimize a certain error bound. It is interesting though to point out that several researchers have used the direct minimization approach in a local manner. For example, Bank and Smith [3] minimize an interpolation or a posteriori error estimate for linear finite elements using a Gauss–Seidel-like iterative method, in which sweeps are run through the vertices, locally optimizing the position of a single vertex while all others being held fixed. A similar method has been used by Tourigny and Baines [27], Tourigny and Hülsemann [28], and Baines and Leary [2] for minimizing the L_2 norm of the residual of partial differential equations.

4. Monitor functions

We define in this section the monitor function using the results obtained in the preceding section. According to (29), (31), and (33), we consider two types of monitor functions, scalar (Winslow's type) and non-scalar matrices. (Recall that a scalar matrix is the product of a scalar function with the identity matrix.) Following common practice, we choose the monitor function to be symmetric and positive definite. (The necessity of the positiveness for the non-singularity of the coordinate transformation can be easily seen from the equidistribution criterion (8).) It is emphasized that we seek the coordinate transformation to bound rather than minimize the functional B_1, B_2, or B_3.

4.1. Winslow's type of monitor functions

Consider the estimate (29). To define a positive definite G, we replace B_1 with functional

$$\begin{aligned}\tilde{B}_1[\xi] &= \int_\Omega \frac{1}{J^{2m}}\left(\operatorname{tr}(\boldsymbol{J}^{\mathrm{T}}\boldsymbol{J})\right)^{k+1+m(n-1)}\left(\alpha + \|\partial^{k+1}v\|_F^2\right)\mathrm{d}\boldsymbol{x}\\ &= \alpha\int_\Omega \frac{1}{J^{2m}}\left(\operatorname{tr}(\boldsymbol{J}^{\mathrm{T}}\boldsymbol{J})\right)^{k+1+m(n-1)}\left(1+\frac{1}{\alpha}\|\partial^{k+1}v\|_F^2\right)\mathrm{d}\boldsymbol{x},\end{aligned} \tag{37}$$

where $\alpha > 0$, often referred to as the adaptation intensity parameter, is to be determined. The introduction of α provides a mechanism for better control of mesh concentration without damaging the convergence order of estimate (29). The choice of this parameter has been discussed in [4] for the one-dimensional case and [15] for the multi-dimensional case.

We choose the monitor function so that $\tilde{B}_1$ has the form

$$\tilde{B}_1[\xi] = \alpha\int_\Omega \frac{\sqrt{g}}{(J^2 g)m}\left[\operatorname{tr}(\boldsymbol{J}^{\mathrm{T}}G\boldsymbol{J})\right]^{k+1+m(n-1)}\mathrm{d}\boldsymbol{x}. \tag{38}$$

The motivation is that, during the course of error estimation, the regularity condition (see below) will take care of the factor $\operatorname{tr}(\boldsymbol{J}^{\mathrm{T}}G\boldsymbol{J})$ while the equidistribution condition (also see below) takes care of the factor $J\sqrt{g}$. In the end, an estimate independent of the coordinate transformation can be obtained.

Comparing (38) with (37) and keeping in mind that G is defined as a scalar matrix, we obtain

$$\boxed{G = I\left(1+\tfrac{1}{\alpha}\|\partial^{k+1}v\|_F^2\right)^{\frac{2}{2(k+1-m)+n}}} \tag{39}$$

$$\boxed{\sqrt{g} = \left(1+\tfrac{1}{\alpha}\|\partial^{k+1}v\|_F^2\right)^{\frac{n}{2(k+1-m)+n}}} \tag{40}$$

We now proceed with estimating B_1. Recall that functional (11) has been formulated so that its minimization tends to make the eigenvalues of $\boldsymbol{J}^{-1}G^{-1}\boldsymbol{J}^{-\mathrm{T}}$ to be equal and the function $J\sqrt{g}$ to be constant. It is thus reasonable to assume that the coordinate transformation or mesh generated through the functional $I[\xi]$ satisfies the (solution-dependent) regularity condition

$$\left[\frac{\operatorname{tr}(\boldsymbol{J}^{\mathrm{T}}G\boldsymbol{J})}{n\det(\boldsymbol{J}^{\mathrm{T}}G\boldsymbol{J})^{\frac{1}{n}}}\right]^{\frac{n}{2}} \leqslant C_{\mathrm{iso}} \quad \forall \boldsymbol{x}\in\Omega, \tag{41}$$

and the equidistribution condition

$$\frac{J\sqrt{g}}{\sigma} \leqslant C_{\text{ep}} \quad \forall x \in \Omega, \tag{42}$$

where C_{iso} and C_{ep} are constants and σ is defined in (9). One may notice that $J\sqrt{g}$ is required to be bounded from above only (rather than to be close to one). Moreover, the form of (41) is chosen in order to be able to replace $\text{tr}(\boldsymbol{J}^{\text{T}}G\boldsymbol{J})$ with $J\sqrt{g}$ under the regularity condition.

Theorem 4.1. *For some integers m and k*: $0 \leqslant m \leqslant k+1$, *assume that the coordinate transformation satisfies the conditions* (41) *and* (42) *with the monitor function defined in* (39). *Then, the interpolation error is bounded by*

$$|v - \Pi v|_m^2 \lesssim Ch_c^{2(k+1-m)} \left[\int_\Omega \left(\alpha + \|\partial^{k+1} v\|_F^2 \right)^{\frac{n}{2(k+1-m)+n}} \mathrm{d}\boldsymbol{x} \right]^{\frac{2(k+1-m)+n}{n}} \quad \forall v \in H^{k+1}(\Omega), \tag{43}$$

where $C = C(C_{\text{iso}}, C_{\text{ep}})$ *is proportional to* $C_{\text{iso}}^{2(k+1-m+mn)/n} C_{\text{ep}}^{2(k+1-m)/n}$.

Proof. From (37), we have

$$\begin{aligned}
\tilde{B}_1[\xi] &= \alpha \int_\Omega \frac{\sqrt{g}}{(J^2 g)^m} \left[\text{tr}(\boldsymbol{J}^{\text{T}} G \boldsymbol{J}) \right]^{k+1+m(n-1)} \mathrm{d}\boldsymbol{x} \\
&\leqslant \alpha C C_{\text{iso}}^{\frac{2(k+1-m+mn)}{n}} \int_\Omega \frac{\sqrt{g}}{(J^2 g)^m} \left[\det(\boldsymbol{J}^{\text{T}} G \boldsymbol{J}) \right]^{\frac{(k+1+m(n-1))}{n}} \mathrm{d}\boldsymbol{x} \quad \text{(using (41))} \\
&= \alpha C C_{\text{iso}}^{\frac{2(k+1-m+mn)}{n}} \int_\Omega \sqrt{g} \left(J^2 g \right)^{\frac{(k+1-m)}{n}} \mathrm{d}\boldsymbol{x} \\
&\leqslant \alpha C C_{\text{iso}}^{\frac{2(k+1-m+mn)}{n}} C_{\text{ep}}^{\frac{2(k+1-m)}{n}} \int_\Omega \sqrt{g} \sigma^{\frac{2(k+1-m)}{n}} \mathrm{d}\boldsymbol{x} \quad \text{(using (42))} \\
&\leqslant \alpha C C_{\text{iso}}^{\frac{2(k+1-m+mn)}{n}} C_{\text{ep}}^{\frac{2(k+1-m)}{n}} \sigma^{\frac{2(k+1-m)+n}{n}}.
\end{aligned}$$

The conclusion follows from (9), (29), (40), and the fact that $B_1[\xi] \leqslant \tilde{B}_1[\xi]$. □

The theorem shows that the error bound depends continuously on C_{iso} and C_{ep}. In the meantime, this dependence is moderate in the sense that the powers of the constants, $2(k+1-m+mn)/n$ and $2(k+1-m)/n$, are small or moderate, especially when low degree interpolation polynomials are used (as is in many practical computations).

4.1.1. Optimality of the monitor function

Generally speaking, it is difficult to make precise comparison of the bound (43) with the classic result (14) on a uniform mesh. This is because the constant C in (43) depends on C_{iso} and C_{ep} and can be considerably different from that in (14). On the other hand, (43) has a smaller solution-dependent factor than that given in (14), i.e.,

$$\left[\int_\Omega \left(\alpha + \|\partial^{k+1} v\|_F^2 \right)^{\frac{n}{2(k+1-m)+n}} \mathrm{d}\boldsymbol{x} \right]^{\frac{2(k+1-m)+n}{n}} \leqslant \int_\Omega \left(\alpha + \|\partial^{k+1} v\|_F^2 \right) \mathrm{d}\boldsymbol{x} \tag{44}$$

and the right-hand side is comparable to $|v|_{k+1}^2$ if $\alpha \leqslant \int_\Omega \|\partial^{k+1} v\|_F^2 \, \mathrm{d}\boldsymbol{x}$. When $\partial^{k+1} v$ is sufficiently smooth, the two sides of (44) are comparable, and uniform and adaptive meshes having the same number of nodes will produce similar results. However, when $\partial^{k+1} v$ is rough, the right-hand side of (44) can become much larger than the left-hand side, and an adaptive mesh will produce much more accurate results than a uniform mesh does.

Recall that the purpose of mesh adaptation is to obtain accurate resolution of rough functions. (In the current circumstance, the roughness can be measured by the ratio of the right-hand side to the left-hand side of (44) with α being set to be zero.) For the sake of simplicity, we assume hereafter that we are always dealt with rough functions and thus consider only solution-dependent factors when comparing error bounds or studying their optimality.

By construction, (39) leads to the smallest error bound (43). (In this sense, (39) is the optimal monitor function.) To explain this, we consider as an example the widely used monitor function

$$G = I\left(1+\frac{1}{\alpha}|\nabla v|^2\right)^{\frac{1}{n}}, \quad \sqrt{g} = \left(1+\frac{1}{\alpha}|\nabla v|^2\right)^{\frac{1}{2}} \tag{45}$$

that corresponds to the piecewise constant interpolation $(k,m) = (0,0)$. Under the conditions (41) and (42), an error estimate can be obtained from (29) as

$$\|v - \Pi v\|^2 \lesssim Ch_c^2\left[\int_\Omega \left(\alpha+|\nabla v|^2\right)^{\frac{1}{2}} \mathrm{d}\boldsymbol{x}\right]^{\frac{2}{n}} \int_\Omega \left(\alpha+|\nabla v|^2\right)^{\frac{n-1}{n}} \mathrm{d}\boldsymbol{x}. \tag{46}$$

On the other hand, for the case $(k,m) = (0,0)$ estimate (43) reads as

$$\|v - \Pi v\|^2 \lesssim Ch_c^2\left[\int_\Omega \left(\alpha+|\nabla v|^2\right)^{\frac{n}{2+n}} \mathrm{d}\boldsymbol{x}\right]^{\frac{2+n}{n}}. \tag{47}$$

It is not difficult to show

$$\left[\int_\Omega \left(\alpha+|\nabla v|^2\right)^{\frac{n}{2+n}} \mathrm{d}\boldsymbol{x}\right]^{\frac{2+n}{n}} \leqslant \left[\int_\Omega \left(\alpha+|\nabla v|^2\right)^{\frac{1}{2}} \mathrm{d}\boldsymbol{x}\right]^{\frac{2}{n}} \int_\Omega \left(\alpha+|\nabla v|^2\right)^{\frac{n-1}{n}} \mathrm{d}\boldsymbol{x}$$

and thus (46) has a larger bound than that in (47).

It is interesting to note that the difference between bounds (47) and (46) for adaptive meshes is not as great as the difference between bound (47) for an adaptive mesh and bound (14) for a uniform mesh. To see this more clearly, (46) can be enlarged as

$$\|v - \Pi v\|^2 \lesssim Ch_c^2\left[\int_\Omega \left(\alpha+|\nabla v|^2\right)^{\frac{n-1}{n}} \mathrm{d}\boldsymbol{x}\right]^{\frac{n}{n-1}}. \tag{48}$$

Thus, the solution-dependent factors involved in the interpolation error bounds associated with the optimal monitor function (39), the monitor function (45), and a uniform mesh are given, respectively, by

$$\left[\int_\Omega \left(\alpha+|\nabla v|^2\right)^{\frac{1}{2}} \mathrm{d}\boldsymbol{x}\right]^2, \quad \left[\int_\Omega \left(\alpha+|\nabla v|^2\right)^{\frac{1}{2}} \mathrm{d}\boldsymbol{x}\right]^2, \quad \int_\Omega |\nabla v|^2 \mathrm{d}\boldsymbol{x}$$

for $n = 2$ and

$$\left[\int_\Omega \left(\alpha+|\nabla v|^2\right)^{\frac{3}{5}} \mathrm{d}\boldsymbol{x}\right]^{\frac{5}{3}}, \quad \left[\int_\Omega \left(\alpha+|\nabla v|^2\right)^{\frac{2}{3}} \mathrm{d}\boldsymbol{x}\right]^{\frac{3}{2}}, \quad \int_\Omega |\nabla v|^2 \mathrm{d}\boldsymbol{x}$$

for $n = 3$. The above observation, together with the fact that the interpolation error bound depends continuously on C_{iso} and C_{ep}, indicates that estimate (43) is rather stable under perturbations to the optimal mesh distribution resulting from the monitor function (39). This conclusion is consistent with the observations made by Babuska and Rheinboldt [1] and de Boor [10] for one-dimensional problems. The conclusion also explains why many existing methods have some degree of success although they may not produce optimal adaptive meshes.

4.1.2. Choice of the intensity parameter

The intensity parameter α should not be chosen either too small or too large. Too small α leads to an over-concentrated and possibly very skewed mesh, whereas too large α results in a uniform mesh. The following two guidelines can be used for the choice of α. The first is to make G invariant under the scaling transformation of v. In this way, a simple multiplication of v by a constant will not affect mesh concentration. Moreover, a dimensionless G makes it easier and more efficient to find a minimizer of $I[\boldsymbol{\xi}]$ numerically. The other guideline is to have a sufficient number of mesh points concentrated in the region of large $\sqrt{g}$. To this end, we recall from (42) that $\sqrt{g}$ is proportional to the mesh density $1/J$. Thus, $(\int_\Omega \sqrt{g}\,\mathrm{d}\boldsymbol{x} - \int_\Omega \mathrm{d}\boldsymbol{x})/\int_\Omega \sqrt{g}\,\mathrm{d}\boldsymbol{x}$ is a good indicator of the percent of the mesh points concentrated in the region of large $\sqrt{g}$. Define

$$\Omega' \equiv \left\{\boldsymbol{x} | \sqrt{g(\boldsymbol{x})} \approx 1\right\}, \quad \Omega'' \equiv \Omega \setminus \Omega' = \left\{\boldsymbol{x} | \sqrt{g(\boldsymbol{x})} \gg 1\right\}. \tag{49}$$

Then

$$\int_{\Omega'} (\sqrt{g} - 1)\,\mathrm{d}\boldsymbol{x} \approx 0, \quad \int_{\Omega'} \sqrt{g}\,\mathrm{d}\boldsymbol{x} + \int_{\Omega''} \mathrm{d}\boldsymbol{x} \approx |\Omega|.$$

We have

$$\begin{aligned}\frac{\int_\Omega (\sqrt{g} - 1)\,\mathrm{d}\boldsymbol{x}}{\int_\Omega \sqrt{g}\,\mathrm{d}\boldsymbol{x}} &= \frac{\int_{\Omega'} (\sqrt{g} - 1)\,\mathrm{d}\boldsymbol{x} + \int_{\Omega''} (\sqrt{g} - 1)\,\mathrm{d}\boldsymbol{x}}{\int_{\Omega'} (\sqrt{g})\,\mathrm{d}\boldsymbol{x} + \int_{\Omega''} \mathrm{d}\boldsymbol{x} + \int_{\Omega''} (\sqrt{g} - 1)\,\mathrm{d}\boldsymbol{x}} \approx \frac{\int_{\Omega''} (\sqrt{g} - 1)\,\mathrm{d}\boldsymbol{x}}{|\Omega| + \int_{\Omega''} (\sqrt{g} - 1)\,\mathrm{d}\boldsymbol{x}} \\ &= \left[1 + \frac{|\Omega|}{\int_{\Omega''} (\sqrt{g} - 1)\,\mathrm{d}\boldsymbol{x}}\right]^{-1}. \end{aligned} \tag{50}$$

We choose α such that

$$\int_{\Omega''} (\sqrt{g} - 1)\,\mathrm{d}\boldsymbol{x} \approx |\Omega|, \tag{51}$$

i.e., about 50% of the mesh points are concentrated on Ω''.

From (40), Ω' and Ω'' can be characterized as

$$\Omega' = \{\boldsymbol{x} \mid \|\partial^{k+1} v\|_F^2 \ll \alpha\} \quad \text{and} \quad \Omega'' = \{\boldsymbol{x} \mid \|\partial^{k+1} v\|_F^2 \gg \alpha\},$$

respectively. Thus,

$$\int_{\Omega''} (\sqrt{g} - 1)\,\mathrm{d}\boldsymbol{x} \approx \int_{\Omega''} \left(\frac{1}{\alpha} \|\partial^{k+1} v\|_F^2\right)^{\frac{n}{2(k+1-m)+n}} \mathrm{d}\boldsymbol{x}.$$

From (51), α should be defined such that

$$\alpha^{\frac{n}{2(k+1-m)+n}} \approx \frac{1}{|\Omega|} \int_{\Omega''} \|\partial^{k+1} v\|_F^{\frac{2n}{2(k+1-m)+n}} \mathrm{d}\boldsymbol{x}. \tag{52}$$

This suggests

$$\boxed{\alpha = \left[\frac{1}{|\Omega|} \int_\Omega \|\partial^{k+1} v\|_F^{\frac{2n}{2(k+1-m)+n}} \mathrm{d}\boldsymbol{x}\right]^{\frac{2(k+1-m)+n}{n}}} \tag{53}$$

for the monitor function (39). It is easy to verify that with this definition of α, the monitor function G and its determinant g are invariant under the scaling transformation of v. To see if (52) is true, from the definitions of Ω' and α we get

$$\frac{1}{|\Omega|}\int_{\Omega'}\|\partial^{k+1}v\|_F^{\frac{2n}{2(k+1-m)+n}}\,\mathrm{d}\boldsymbol{x}\ll\alpha^{\frac{n}{2(k+1-m)+n}}=\frac{1}{|\Omega|}\int_{\Omega'}\|\partial^{k+1}v\|_F^{\frac{2n}{2(k+1-m)+n}}\,\mathrm{d}\boldsymbol{x}+\frac{1}{|\Omega|}\int_{\Omega''}\|\partial^{k+1}v\|_F^{\frac{2n}{2(k+1-m)+n}}\,\mathrm{d}\boldsymbol{x}.$$

Thus,

$$\frac{1}{|\Omega|}\int_{\Omega'}\|\partial^{k+1}v\|_F^{\frac{2n}{2(k+1-m)+n}}\,\mathrm{d}\boldsymbol{x}\ll\frac{1}{|\Omega|}\int_{\Omega''}\|\partial^{k+1}v\|_F^{\frac{2n}{2(k+1-m)+n}}\,\mathrm{d}\boldsymbol{x}$$

and (52) holds.

It is interesting to point out the similarity between the definition of α (53) and the solution dependent factor in (43). With (53), we can readily show

$$\left[\int_\Omega\left(\alpha+\|\partial^{k+1}v\|_F^2\right)^{\frac{n}{2(k+1-m)+n}}\mathrm{d}\boldsymbol{x}\right]^{\frac{2(k+1-m)+n}{n}}\leqslant C\left[\int_\Omega\|\partial^{k+1}v\|_F^{\frac{2n}{2(k+1-m)+n}}\mathrm{d}\boldsymbol{x}\right]^{\frac{2(k+1-m)+n}{n}}.$$

Thus, (43) can be written as

$$|v-\Pi v|_m^2\lesssim Ch_c^{2(k+1-m)}\left[\int_\Omega\|\partial^{k+1}v\|_F^{\frac{2n}{2(k+1-m)+n}}\mathrm{d}\boldsymbol{x}\right]^{\frac{2(k+1-m)+n}{n}}\quad\forall v\in H^{k+1}(\Omega).\tag{54}$$

It is remarked that mesh concentration can be adjusted by modifying the definition of α, viz.,

$$\alpha=\left[\frac{(1-\beta)}{\beta|\Omega|}\int_\Omega\|\partial^{k+1}v\|_F^{\frac{2n}{2(k+1-m)+n}}\mathrm{d}\boldsymbol{x}\right]^{\frac{2(k+1-m)+n}{n}},$$

where $\beta\in(0,1)$ represents the percent of the mesh points concentrated in Ω''; see [15].

4.1.3. Regularity condition

Recall that λ_i's are the eigenvalues of matrix $\boldsymbol{J}^{-1}G^{-1}\boldsymbol{J}^{-\mathrm{T}}$. Let $\mu_i=\lambda^{-1}$, $i=1,\ldots,n$. Denote $\mu_{\min}=\min_i\mu_i$ and $\mu_{\max}=\max_i\mu_i$. Then regularity condition (41) can be rewritten as

$$\frac{1}{n}\sum_i\mu_i\leqslant C_{\mathrm{iso}}^{\frac{2}{n}}\left(\prod_i\mu_i\right)^{\frac{1}{n}}.\tag{55}$$

Lemma 4.1. *Regularity condition* (41) *implies*

$$\mu_{\min}\geqslant\left[\sqrt{n(n-1)(C_{\mathrm{iso}}^{\frac{2}{n}}-1)}+1\right]^{-2n}\mu_{\max}.$$

Proof. From the refined version of the arithmetic-mean geometric-mean inequality (cf. (5)) we have

$$\frac{1}{n(n-1)}\sum_{i<j}\left(\sqrt{\mu_i}-\sqrt{\mu_j}\right)^2\leqslant\frac{1}{n}\sum_i\mu_i-\left(\prod_i\mu_i\right)^{\frac{1}{n}}.$$

The result of the lemma follows from (55) and that

$$\begin{aligned}C_{\mathrm{iso}}^{\frac{2}{n}}-1&\geqslant\frac{1}{n(n-1)}\cdot\frac{\sum_{i<j}\left(\sqrt{\mu_i}-\sqrt{\mu_j}\right)^2}{\left(\prod_i\mu_i\right)^{\frac{1}{n}}}\geqslant\frac{1}{n(n-1)}\cdot\frac{\left(\sqrt{\mu_{\max}}-\sqrt{\mu_{\min}}\right)^2}{\mu_{\max}^{\frac{n-1}{n}}\mu_{\min}^{\frac{1}{n}}}\\&\geqslant\frac{1}{n(n-1)}\left[\left(\frac{\mu_{\max}}{\mu_{\min}}\right)^{\frac{1}{2n}}-\left(\frac{\mu_{\min}}{\mu_{\max}}\right)^{\frac{n-1}{2n}}\right]^2\geqslant\frac{1}{n(n-1)}\left[\left(\frac{\mu_{\max}}{\mu_{\min}}\right)^{\frac{1}{2n}}-1\right]^2.\end{aligned}$$

□

We recall that functional $I[\xi]$ in (11) is constructed based on the eigenvalues λ_i's. It is thus natural to ask if (41) implies that

$$\frac{\operatorname{tr}(\boldsymbol{J}^{-1}G^{-1}\boldsymbol{J}^{-\mathrm{T}})}{n\det(\boldsymbol{J}^{-1}G^{-1}\boldsymbol{J}^{-\mathrm{T}})^{\frac{1}{n}}} \leqslant \tilde{C}_{\mathrm{iso}} \quad \forall x \in \Omega$$

for some constant $\tilde{C}_{\mathrm{iso}}$. In fact, from Lemma 4.1 it is not difficult to show that the above inequality holds with

$$\tilde{C}_{\mathrm{iso}} = \left[\sqrt{n(n-1)(C_{\mathrm{iso}}^{\frac{2}{n}}-1)}+1\right]^{2n}.$$

For the current situation, (41) is no more than the standard requirement for mesh regularity. Indeed, for a scalar matrix G,

$$\frac{\operatorname{tr}(\boldsymbol{J}^{\mathrm{T}}G\boldsymbol{J})}{n\big(\det(\boldsymbol{J}^{\mathrm{T}}G\boldsymbol{J})\big)^{\frac{1}{n}}} = \frac{\operatorname{tr}(\boldsymbol{J}^{\mathrm{T}}\boldsymbol{J})}{n\big(\det(\boldsymbol{J}^{\mathrm{T}}\boldsymbol{J})\big)^{\frac{1}{n}}}.$$

Thus, according to this measure, an isotropic mesh satisfying (41) with $C_{\mathrm{iso}} = 1$ contains only equilateral cells.

For convenience, we list in Table 1 the optimal monitor functions of Winslow's type and their related information for piecewise constant ($k = 0$) and piecewise linear ($k = 1$) interpolation. It is easy to see that for each pair of (k, m), both G and $\sqrt{g}$ and therefore mesh concentration are dimension dependent (i.e. their forms are different in different dimensions).

It is remarked that the one-dimensional version of monitor function (39) is basically the same as those proposed by Carey and Dinh [7] (also see [8]). The only difference is that the current monitor function is floored by the intensity parameter α.

4.2. Non-scalar matrix monitor functions

Non-scalar matrix monitor functions are considered only for the piecewise constant ($k = 0$) and piecewise linear ($k = 1$) interpolation.

Table 1
Monitor functions of Winslow's type for piecewise constant and piecewise linear interpolation

k	m	Dim	G	$\sqrt{g} \propto 1/J$	Error order
0	0	1D	$(1+\frac{1}{\alpha}\lvert v'\rvert^2)^{2/3}$	$(1+\frac{1}{\alpha}\lvert v'\rvert^2)^{1/3}$	$O(h_c)$ in $\lVert\cdot\rVert$
		2D	$I(1+\frac{1}{\alpha}\lvert\nabla v\rvert^2)^{1/2}$	$(1+\frac{1}{\alpha}\lvert\nabla v\rvert^2)^{1/2}$	
		3D	$I(1+\frac{1}{\alpha}\lvert\nabla v\rvert^2)^{2/5}$	$(1+\frac{1}{\alpha}\lvert\nabla v\rvert^2)^{3/5}$	
1	0	1D	$(1+\frac{1}{\alpha}\lvert v''\rvert^2)^{2/5}$	$(1+\frac{1}{\alpha}\lvert v''\rvert^2)^{1/5}$	$O(h_c^2)$ in $\lVert\cdot\rVert$
		2D	$I(1+\frac{1}{\alpha}\lVert H\rVert_F^2)^{1/3}$	$(1+\frac{1}{\alpha}\lVert H\rVert_F^2)^{1/3}$	
		3D	$I(1+\frac{1}{\alpha}\lVert H\rVert_F^2)^{2/7}$	$(1+\frac{1}{\alpha}\lVert H\rVert_F^2)^{3/7}$	
1	1	1D	$(1+\frac{1}{\alpha}\lvert v''\rvert^2)^{2/3}$	$(1+\frac{1}{\alpha}\lvert v''\rvert^2)^{1/3}$	$O(h_c)$ in $\lvert\cdot\rvert_1$
		2D	$I(1+\frac{1}{\alpha}\lVert H\rVert_F^2)^{1/2}$	$(1+\frac{1}{\alpha}\lVert H\rVert_F^2)^{1/2}$	
		3D	$I(1+\frac{1}{\alpha}\lVert H\rVert_F^2)^{2/5}$	$(1+\frac{1}{\alpha}\lVert H\rVert_F^2)^{3/5}$	

The definition of the intensity parameter α is given in (53).

4.2.1. Piecewise constant interpolation

In this case we have $(k,m)=(0,0)$ and the corresponding error estimate is given in (31). Introduce a new functional as

$$\tilde{B}_2[\xi]=\alpha\int_\Omega \operatorname{tr}\left(\boldsymbol{J}^{\mathrm{T}}\left(I+\frac{1}{\alpha}\nabla v(\nabla v)^{\mathrm{T}}\right)\boldsymbol{J}\right)\mathrm{d}\boldsymbol{x}. \tag{56}$$

The monitor function is defined such that $\tilde{B}_2$ can be written in the form

$$\tilde{B}_2[\xi]=\alpha\int_\Omega \sqrt{g}\operatorname{tr}(\boldsymbol{J}^{\mathrm{T}}G\boldsymbol{J})\,\mathrm{d}\boldsymbol{x}. \tag{57}$$

It is easy to get

$$\boxed{G=\left(I+\tfrac{1}{\alpha}\nabla v\nabla v^{\mathrm{T}}\right)\cdot\left(1+\tfrac{1}{\alpha}|\nabla v|^2\right)^{-\frac{1}{n+2}}} \tag{58}$$

and

$$\boxed{\sqrt{g}=\left(1+\tfrac{1}{\alpha}|\nabla v|^2\right)^{\frac{1}{n+2}}} \tag{59}$$

The intensity parameter is chosen as

$$\boxed{\alpha=\left[\tfrac{1}{|\Omega|}\int_\Omega|\nabla v|^{\frac{2}{n+2}}\mathrm{d}\boldsymbol{x}\right]^{n+2}} \tag{60}$$

Theorem 4.2. *Assume that the coordinate transformation satisfies the conditions* (41) *and* (42) *with the monitor function defined in* (58) *and* α *defined in* (60). *Then, error for piecewise constant interpolation is bounded by*

$$\|v-\Pi v\|^2\lesssim Ch_{\mathrm{c}}^2\left[\int_\Omega|\nabla v|^{\frac{2}{n+2}}\mathrm{d}\boldsymbol{x}\right]^{n+2}\quad\forall v\in H^1(\Omega), \tag{61}$$

where $C=C(C_{\mathrm{iso}},C_{\mathrm{ep}})$ *is proportional to* $(C_{\mathrm{iso}}C_{\mathrm{ep}})^{\frac{2}{n}}$.

We note that for the case $(k,m)=(0,0)$, the estimate (54) associated with a Winslow-type monitor function reads as

$$\|v-\Pi v\|^2\lesssim Ch_{\mathrm{c}}^2\left[\int_\Omega|\nabla v|^{\frac{2n}{n+2}}\mathrm{d}\boldsymbol{x}\right]^{\frac{n+2}{n}}.$$

By comparing this with (61), we can see that a Winslow-type monitor function leads a larger bound than a non-scalar matrix monitor function, provided that the resulting meshes satisfy the regularity and equidistribution conditions.

In the current situation, the mesh isotropy measure has a different geometric meaning from that using Winslow-type monitor functions. Indeed, (41) reads as

$$\frac{\operatorname{tr}(\boldsymbol{J}^{\mathrm{T}}\left(I+\frac{1}{\alpha}\nabla v\nabla v^{\mathrm{T}}\right)\boldsymbol{J})}{n\left(\det(\boldsymbol{J}^{\mathrm{T}}\left(I+\frac{1}{\alpha}\nabla v\nabla v^{\mathrm{T}}\right)\boldsymbol{J})\right)^{\frac{1}{n}}}\leqslant C_{\mathrm{iso}}^{\frac{2}{n}}. \tag{62}$$

According to this measure, an isotropic mesh (with $C_{\rm iso} = 1$) is allowed to have non-equilateral cells.

The matrix monitor function based on gradient of v,

$$G = I + \frac{1}{\alpha}\nabla v \nabla v^{\rm T}, \quad \sqrt{g} = \sqrt{1 + \frac{1}{\alpha}|\nabla v|^2} \tag{63}$$

has been used in the past because of its similarity to the one-dimensional arc-length monitor function. If we choose the intensity parameter as

$$\alpha = \left[\frac{1}{|\Omega|}\int_\Omega |\nabla v|\,{\rm d}\boldsymbol{x}\right]^2$$

and assume that the resulting mesh satisfies (41) and (42), we can get

$$\|v - \Pi v\|^2 \lesssim C h_{\rm c}^2 \left[\int_\Omega |\nabla v|\,{\rm d}\boldsymbol{x}\right]^2, \tag{64}$$

which gives an error bound greater than that given in (61).

4.2.2. Piecewise linear interpolation

In this case we have $k = 1$ and $m = 0$ or 1. The corresponding error estimate is given in (33). The new functional can be introduced as

$$\begin{aligned}\tilde{B}_3[\xi] &= \alpha^2 \int_\Omega \frac{1}{J^{2m}} \cdot \left[{\rm tr}\left(\boldsymbol{J}^{\rm T}\boldsymbol{J}\right)\right]^{m(n-1)} \left[{\rm tr}\left(\boldsymbol{J}^{\rm T}\left(I + \frac{1}{\alpha}|H|\right)\boldsymbol{J}\right)\right]^2 {\rm d}\boldsymbol{x} \\ &= \alpha^2 \int_\Omega \frac{1}{J^{\frac{2m}{n}}} \cdot \left[\frac{{\rm tr}(\boldsymbol{J}^{\rm T}\boldsymbol{J})}{J^{\frac{2}{n}}}\right]^{m(n-1)} \left[{\rm tr}\left(\boldsymbol{J}^{\rm T}\left(I + \frac{1}{\alpha}|H|\right)\boldsymbol{J}\right)\right]^2 {\rm d}\boldsymbol{x}.\end{aligned} \tag{65}$$

Rewriting it into the form

$$\tilde{B}_3[\xi] = \alpha^2 \int_\Omega \frac{\sqrt{g}}{(J^2 g)^{\frac{m}{n}}} \left[\frac{{\rm tr}(\boldsymbol{J}^{\rm T}\boldsymbol{J})}{J^{\frac{2}{n}}}\right]^{m(n-1)} \left[{\rm tr}\left(\boldsymbol{J}^{\rm T} G \boldsymbol{J}\right)\right]^2 {\rm d}\boldsymbol{x}, \tag{66}$$

one can obtain

$$\boxed{G = \left(I + \tfrac{1}{\alpha}|H|\right) \cdot \det\left(I + \tfrac{1}{\alpha}|H|\right)^{\frac{2m-n}{n(n-2m+4)}}} \tag{67}$$

and

$$\boxed{\sqrt{g} = \det\left(I + \tfrac{1}{\alpha}|H|\right)^{\frac{2}{n-2m+4}}} \tag{68}$$

The form of (66) suggests that the following new regularity assumption be used,

$$\left[\frac{{\rm tr}\left(\boldsymbol{J}^{\rm T}\boldsymbol{J}\right)}{n J^{\frac{2}{n}}}\right]^{\frac{m(n-1)}{2}} \left[\frac{{\rm tr}\left(\boldsymbol{J}^{\rm T} G \boldsymbol{J}\right)}{n \det\left(\boldsymbol{J}^{\rm T} G \boldsymbol{J}\right)^{\frac{1}{n}}}\right] \leqslant C_{\rm iso}^{\frac{2}{n}}. \tag{69}$$

This condition is different from (41) for $m \neq 0$. Like the case of piecewise constant interpolation, an isotropic mesh satisfying the above condition with $C_{\rm iso} = 1$ will generally contain non-equilateral cells. For the present case, α cannot be separated out from $\det(I + (1/\alpha)|H|)$ without significantly enlarging the estimate. For this reason, α is defined implicitly as

$$\boxed{\int_\Omega \det\left(I + \tfrac{1}{\alpha}|H|\right)^{\frac{2}{n-2m+4}} {\rm d}\boldsymbol{x} = |\Omega| \cdot 2^{1+\max\{\frac{2n}{n-2m+4}-1,0\}}} \tag{70}$$

Note that the existence of α is guaranteed as long as $\int_\Omega [\mathrm{tr}(|H|)]^{n/(n-2m+4)}\,\mathrm{d}\boldsymbol{x} > 0$. The form of (70) is motivated by the discussion on the choice of α in Section 4.1.2, the desire that $\sigma \equiv \int_\Omega \sqrt{g}\,\mathrm{d}\boldsymbol{x}$ is bounded by a constant independent of v, and the following derivation of a bound of α. In fact, from (70) we have

$$\begin{aligned}
2|\Omega| &\leqslant 2^{-\max\{\frac{2n}{n-2m+4}-1,0\}} \int_\Omega \left(\frac{1}{n}\mathrm{tr}\left(I+\frac{1}{\alpha}|H|\right)\right)^{\frac{2n}{n-2m+4}} \mathrm{d}\boldsymbol{x} \\
&\leqslant 2^{-\max\{\frac{2n}{n-2m+4}-1,0\}} \int_\Omega \left(1+\frac{1}{n\alpha}\mathrm{tr}(|H|)\right)^{\frac{2n}{n-2m+4}} \mathrm{d}\boldsymbol{x} \\
&\leqslant |\Omega| + \alpha^{-\frac{2n}{n-2m+4}} \int_\Omega \left(\frac{1}{n}\mathrm{tr}(|H|)\right)^{\frac{2n}{n-2m+4}} \mathrm{d}\boldsymbol{x}.
\end{aligned}$$

Thus,

$$\alpha \leqslant \left[\frac{1}{|\Omega|}\int_\Omega \left(\frac{1}{n}\mathrm{tr}(|H|)\right)^{\frac{2n}{n-2m+4}} \mathrm{d}\boldsymbol{x}\right]^{\frac{n-2m+4}{2n}}. \tag{71}$$

Theorem 4.3. *For $m = 0$ or $m = 1$, assume that the coordinate transformation satisfies the conditions* (69) *and* (42) *with the monitor function defined in* (67) *and α defined in* (70). *Then, the error for piecewise linear interpolation is bounded by*

$$|v - \Pi v|_m^2 \lesssim C\alpha^2 h_c^{2(2-m)} \quad \forall v \in H^2(\Omega), \tag{72}$$

where $C = C(C_{\mathrm{iso}}, C_{\mathrm{ep}})$ is proportional to $C_{\mathrm{iso}}^{4/n} C_{\mathrm{ep}}^{(4-2m)/n}$.

We now consider a non-optimal monitor function

$$G = I + \frac{1}{\alpha}|H|, \quad \sqrt{g} = \det\left(I+\frac{1}{\alpha}|H|\right)^{\frac{1}{2}}. \tag{73}$$

Assuming that the resultant mesh satisfies (69) and (42), we can obtain from (33) and (65)

$$|v - \Pi v|_m^2 \lesssim C\alpha^2 h_c^{2(2-m)} \left[\int_\Omega \det\left(I+\frac{1}{\alpha}|H|\right)^{\frac{1}{2}} \mathrm{d}\boldsymbol{x}\right]^{\frac{4-2m}{n}} \int_\Omega \det\left(I+\frac{1}{\alpha}|H|\right)^{m/n} \mathrm{d}\boldsymbol{x}, \tag{74}$$

that can be shown to have a bound greater than or equal to that given in (72).

Table 2 lists the matrix monitor functions and related information for piecewise constant and piecewise linear interpolation. Once again, G and $\sqrt{g}$ and therefore mesh concentration are dimension dependent.

Table 2
The non-scalar matrix monitor functions for piecewise constant and linear interpolation

k	m	Dim	G	$\sqrt{g} \propto 1/J$	Error order
0	0	1D	$(1+\frac{1}{\alpha}\lvert v'\rvert^2)^{2/3}$	$(1+\frac{1}{\alpha}\lvert v'\rvert^2)^{1/3}$	$O(h_c)$ in $\lVert\cdot\rVert$
		2D	$\left(I+\frac{1}{\alpha}\nabla v(\nabla v)^{\mathrm{T}}\right)\left(1+\frac{1}{\alpha}\lvert\nabla v\rvert^2\right)^{-1/4}$	$\left(1+\frac{1}{\alpha}\lvert\nabla v\rvert^2\right)^{1/4}$	
		3D	$\left(I+\frac{1}{\alpha}\nabla v(\nabla v)^{\mathrm{T}}\right)\left(1+\frac{1}{\alpha}\lvert\nabla v\rvert^2\right)^{-1/5}$	$\left(1+\frac{1}{\alpha}\lvert\nabla v\rvert^2\right)^{1/5}$	
1	0	1D	$(1+\frac{1}{\alpha}\lvert v''\rvert)^{4/5}$	$(1+\frac{1}{\alpha}\lvert v''\rvert)^{2/5}$	$O(h_c^2)$ in $\lVert\cdot\rVert$
		2D	$\left(I+\frac{1}{\alpha}\lvert H\rvert\right)\det\left(I+\frac{1}{\alpha}\lvert H\rvert\right)^{-1/6}$	$\det\left(I+\frac{1}{\alpha}\lvert H\rvert\right)^{1/3}$	
		3D	$\left(I+\frac{1}{\alpha}\lvert H\rvert\right)\det\left(I+\frac{1}{\alpha}\lvert H\rvert\right)^{-1/7}$	$\det\left(I+\frac{1}{\alpha}\lvert H\rvert\right)^{2/7}$	
1	1	1D	$(1+\frac{1}{\alpha}\lvert v''\rvert)^{4/3}$	$(1+\frac{1}{\alpha}\lvert v''\rvert)^{2/3}$	$O(h_c)$ in $\lvert\cdot\rvert_1$
		2D	$\left(I+\frac{1}{\alpha}\lvert H\rvert\right)$	$\det\left(I+\frac{1}{\alpha}\lvert H\rvert\right)^{1/2}$	
		3D	$\left(I+\frac{1}{\alpha}\lvert H\rvert\right)\det\left(I+\frac{1}{\alpha}\lvert H\rvert\right)^{-1/15}$	$\det\left(I+\frac{1}{\alpha}\lvert H\rvert\right)^{2/5}$	

The intensity parameter α is defined in (70).

5. Numerical experiments

We present in this section two-dimensional numerical results obtained for three examples. Having the roles of dependent and independent variables been interchanged, the two-dimensional Euler–Lagrange equation of functional $I[\xi]$ defined in (11) reads as [16]

$$\begin{aligned}
&\theta\left[a_{11}\frac{\partial^2 \boldsymbol{x}}{\partial \boldsymbol{\xi}^2}+2a_{12}\frac{\partial^2 \boldsymbol{x}}{\partial \boldsymbol{\xi}\partial \eta}+a_{22}\frac{\partial^2 \boldsymbol{x}}{\partial \eta^2}+a_1\frac{\partial \boldsymbol{x}}{\partial \boldsymbol{\xi}}+a_2\frac{\partial \boldsymbol{x}}{\partial \eta}\right]\\
&\quad+\frac{\theta(q-1)}{\beta}\left[B_{11}\frac{\partial^2 \boldsymbol{x}}{\partial \boldsymbol{\xi}^2}+2B_{12}\frac{\partial^2 \boldsymbol{x}}{\partial \boldsymbol{\xi}\partial \eta}+B_{22}\frac{\partial^2 \boldsymbol{x}}{\partial \eta^2}+b_1\frac{\partial \boldsymbol{x}}{\partial \boldsymbol{\xi}}+b_2\frac{\partial \boldsymbol{x}}{\partial \eta}\right]\\
&\quad+\frac{(1-2\theta)(q-1)2^q\sqrt{g}}{\beta^{q-1}(G\boldsymbol{J}\sqrt{g})^q}\left[C_{11}\frac{\partial^2 \boldsymbol{x}}{\partial \boldsymbol{\xi}^2}+2C_{12}\frac{\partial^2 \boldsymbol{x}}{\partial \boldsymbol{\xi}\partial \eta}+C_{22}\frac{\partial^2 \boldsymbol{x}}{\partial \eta^2}+c_1\frac{\partial \boldsymbol{x}}{\partial \boldsymbol{\xi}}+c_2\frac{\partial \boldsymbol{x}}{\partial \eta}\right]=0,
\end{aligned}\tag{75}$$

where $\boldsymbol{x}=(x,y)^{\mathrm{T}}$ and $\boldsymbol{\xi}=(\xi,\eta)^{\mathrm{T}}$ are the physical and computational variables, $\bar{G}=G/g^{1/(2q)}$, $\beta=(\boldsymbol{a}^1)^{\mathrm{T}}\bar{G}^{-1}\boldsymbol{a}^1+(\boldsymbol{a}^2)^{\mathrm{T}}\bar{G}^{-1}\boldsymbol{a}^2$, $J=x_\xi y_\eta-x_\eta y_\xi$, and

$$\boldsymbol{a}_1=\begin{bmatrix}x_\xi\\ y_\xi\end{bmatrix},\quad a_2=\begin{bmatrix}x_\eta\\ y_\eta\end{bmatrix},\quad a^1=\frac{1}{J}\begin{bmatrix}y_\eta\\ -x_\eta\end{bmatrix},\quad a^2=\frac{1}{J}\begin{bmatrix}-y_\xi\\ x_\xi\end{bmatrix}.$$

The coefficients are given by

$$\begin{aligned}
a_{11}&=(\boldsymbol{a}^1)^{\mathrm{T}}\bar{G}^{-1}\boldsymbol{a}^1,\quad a_{12}=(\boldsymbol{a}^1)^{\mathrm{T}}\bar{G}^{-1}\boldsymbol{a}^2,\quad a_{22}=(\boldsymbol{a}^2)^{\mathrm{T}}\bar{G}^{-1}\boldsymbol{a}^2,\\
a_1&=-(\boldsymbol{a}^1)^{\mathrm{T}}\frac{\partial\bar{G}^{-1}}{\partial\boldsymbol{\xi}}\boldsymbol{a}^1-(\boldsymbol{a}^1)^{\mathrm{T}}\frac{\partial\bar{G}^{-1}}{\partial\eta}\boldsymbol{a}^2,\quad a_2=-(\boldsymbol{a}^2)^{\mathrm{T}}\frac{\partial\bar{G}^{-1}}{\partial\boldsymbol{\xi}}\boldsymbol{a}^1-(\boldsymbol{a}^2)^{\mathrm{T}}\frac{\partial\bar{G}^{-1}}{\partial\eta}\boldsymbol{a}^2,\\
B_{11}&=2\left(\bar{G}^{-1}\boldsymbol{a}^1\right)\left(\bar{G}^{-1}\boldsymbol{a}^1\right)^{\mathrm{T}}\left(\boldsymbol{a}^1(\boldsymbol{a}^1)^{\mathrm{T}}+\boldsymbol{a}^1(\boldsymbol{a}^1)^{\mathrm{T}}\right),\\
B_{12}&=\left[\left(\bar{G}^{-1}\boldsymbol{a}^1\right)\left(\bar{G}^{-1}\boldsymbol{a}^2\right)^{\mathrm{T}}+\left(\bar{G}^{-1}\boldsymbol{a}^2\right)\left(\bar{G}^{-1}\boldsymbol{a}^1\right)^{\mathrm{T}}\right]\left(\boldsymbol{a}^1(\boldsymbol{a}^1)^{\mathrm{T}}+\boldsymbol{a}^1(\boldsymbol{a}^1)^{\mathrm{T}}\right),\\
B_{22}&=2\left(\bar{G}^{-1}\boldsymbol{a}^2\right)\left(\bar{G}^{-1}\boldsymbol{a}^2\right)^{\mathrm{T}}\left(\boldsymbol{a}^1(\boldsymbol{a}^1)^{\mathrm{T}}+\boldsymbol{a}^1(\boldsymbol{a}^1)^{\mathrm{T}}\right),\\
b_1&=-(\boldsymbol{a}^1)^{\mathrm{T}}\bar{G}^{-1}\boldsymbol{a}^1\left[(\boldsymbol{a}^1)^{\mathrm{T}}\frac{\partial\bar{G}^{-1}}{\partial\boldsymbol{\xi}}\boldsymbol{a}^1+(\boldsymbol{a}^2)^{\mathrm{T}}\frac{\partial\bar{G}^{-1}}{\partial\boldsymbol{\xi}}\boldsymbol{a}^2\right]\\
&\quad-(\boldsymbol{a}^1)^{\mathrm{T}}\bar{G}^{-1}\boldsymbol{a}^2\left[(\boldsymbol{a}^1)^{\mathrm{T}}\frac{\partial\bar{G}^{-1}}{\partial\eta}\boldsymbol{a}^1+(\boldsymbol{a}^2)^{\mathrm{T}}\frac{\partial\bar{G}^{-1}}{\partial\eta}\boldsymbol{a}^2\right],\\
b_2&=-(\boldsymbol{a}^2)^{\mathrm{T}}\bar{G}^{-1}\boldsymbol{a}^1\left[(\boldsymbol{a}^1)^{\mathrm{T}}\frac{\partial\bar{G}^{-1}}{\partial\boldsymbol{\xi}}\boldsymbol{a}^1+(\boldsymbol{a}^2)^{\mathrm{T}}\frac{\partial\bar{G}^{-1}}{\partial\boldsymbol{\xi}}\boldsymbol{a}^2\right]\\
&\quad-(\boldsymbol{a}^2)^{\mathrm{T}}\bar{G}^{-1}\boldsymbol{a}^2\left[(\boldsymbol{a}^1)^{\mathrm{T}}\frac{\partial\bar{G}^{-1}}{\partial\eta}\boldsymbol{a}^1+(\boldsymbol{a}^2)^{\mathrm{T}}\frac{\partial\bar{G}^{-1}}{\partial\eta}\boldsymbol{a}^2\right],\\
C_{11}&=\boldsymbol{a}_1(a^1)^{\mathrm{T}},\quad C_{12}=\frac{1}{2}\left(\boldsymbol{a}_1(a^2)^{\mathrm{T}}+\boldsymbol{a}_2(a^1)^{\mathrm{T}}\right),\quad C_{22}=\boldsymbol{a}_2(a^2)^{\mathrm{T}},\\
c_1&=\frac{\partial\ln(\sqrt{g})}{\partial\boldsymbol{\xi}},\quad c_2=\frac{\partial\ln(\sqrt{g})}{\partial\eta}.
\end{aligned}\tag{76}$$

Note that the terms in the second square bracket in (75) result from the non-quadratic nature of the functional and those in the third bracket from the equidistribution. In our computations, Ω_c is chosen to be the unit square and the computational mesh is a rectangular mesh. (75) is discretized using central finite differences and solved iteratively with under-relaxation and with the coefficients being calculated at the previous iterate. The linear algebraic system is solved using a preconditioned conjugate gradient method. The converged mesh is obtained when the root-mean-square norm of the residual is less than 10^{-3}. All computations start with a uniform mesh and use a fixed and uniform distribution of boundary points. To show a clear picture of how the variational method works, no smoothing is used for the monitor function. But it should be pointed out that in practice, application of a few sweeps of a low pass filter to the monitor function produces smoother meshes and often leads to more accurate results.

In the presented results, e_0 and e_1 denote the error functions for piecewise constant and linear interpolation, respectively. C_{iso} is defined as

$$C_{\text{iso}} \equiv \max_{(x,y)\in\Omega} \frac{\operatorname{tr}(\boldsymbol{J}^{\mathrm{T}} G \boldsymbol{J})}{2\big(\det(\boldsymbol{J}^{\mathrm{T}} G \boldsymbol{J})\big)^{\frac{1}{2}}} \tag{77}$$

for the cases of Winslow-type monitor functions and non-scalar matrix G with $k = 0$ (piecewise constant interpolation) and

$$C_{\text{iso}} \equiv \max_{(x,y)\in\Omega} \left[\frac{\operatorname{tr}(\boldsymbol{J}^{\mathrm{T}}\boldsymbol{J})}{2J}\right]^{\frac{m}{2}} \cdot \frac{\operatorname{tr}(\boldsymbol{J}^{\mathrm{T}} G \boldsymbol{J})}{2\det\left(\boldsymbol{J}^{\mathrm{T}} G \boldsymbol{J}\right)^{\frac{1}{2}}} \tag{78}$$

for the case of non-scalar matrix G with $k = 1$ (piecewise linear interpolation). C_{ep} is defined as

$$C_{\text{ep}} \equiv \max_{(x,y)\in\Omega} \frac{J\sqrt{g}}{\sigma}, \tag{79}$$

where σ is defined in (9).

Example 1. Our first example is to generate adaptive meshes for

$$v(x,y) = \tanh\left(100((x-1/2)^2 + (y-1/2)^2 - 1/16)\right) \quad (x,y) \in \Omega \equiv (0,1)\times(0,1). \tag{80}$$

Some typical converged adaptive meshes are plotted in Fig. 2. It can be seen that mesh points are concentrated in the correct regions. There is no significant difference between the results using scalar and non-scalar matrix monitor functions for all but the case of piecewise constant interpolation with a non-scalar matrix monitor function.

We list in Table 3 the results obtained using the variational method ($\theta = 0.1$ or 0.5) described in Section 2 with optimal monitor functions for piecewise constant and piecewise linear interpolation. They confirm the theoretical prediction on the convergence order. Specifically, the L^2 norm of the error of piecewise constant interpolation $\|e_0\|$ and the H^1 semi-norm of the error of piecewise linear interpolation $|e_1|_1 = \|\nabla e_1\|$ converges linearly whereas the L^2 norm of the error of piecewise linear interpolation $\|e_1\|$ has quadratic convergence. For all but the case of piecewise constant interpolation $k = 0$ with non-scalar matrix G, we have $C_{\text{iso}} < 3$ and $C_{\text{ep}} < 4$. This shows that the method described in Section 2 is able to generate meshes that satisfy the regularity and the equidistribution conditions (41) and (42) with relatively small constants C_{iso} and C_{ep}.

The results for the case of piecewise constant interpolation ($k = 0$) with a non-scalar matrix monitor function can be explained as follows. For this case, if α is not sufficiently large (and this seems to be the case in our computations),

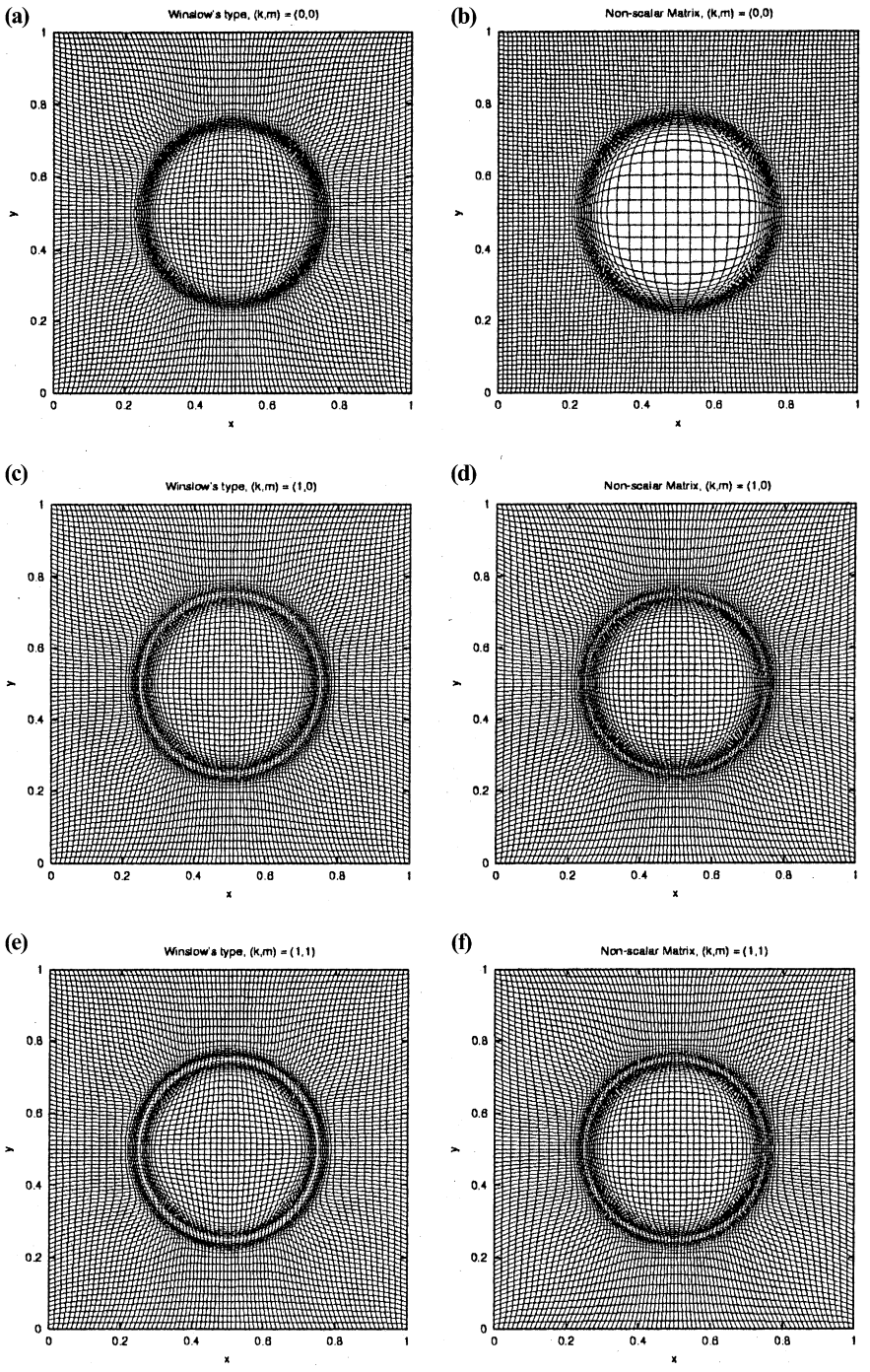

Fig. 2. Converged adaptive meshes of size 81×81 for Example 1 are obtained using the variational method ($\theta = 0.1$) with optimal monitor functions defined for piecewise constant interpolation $(k,m) = (0,0)$ and piecewise linear interpolation $(k,m) = (1,0)$ and $(1,1)$. The left column corresponds to Winslow-type monitor functions while the right column corresponds to non-scalar matrix ones. Rows 1, 2, and 3 correspond to the cases $(k,m) = (0,0),\ (1,0),$ and $(1,1)$, respectively.

Table 3
Interpolation error on adaptive meshes obtained for Example 1 using the variational method ($\theta = 0.1$ or 0.5) with optimal scalar and non-scalar matrix monitor functions for $(k,m) = (0,0)$, (1,0), and (1,1)

θ	$J_{\max}$	Winslow-type G				Non-scalar matrix G			
		$\|e_0\|$	$\|e_0\|_\infty$	C_{iso}	C_{ep}	$\|e_0\|$	$\|e_0\|_\infty$	C_{iso}	C_{ep}
$(k,m) = (0,0)$: *Piecewise constant interpolation*									
0.5	21	7.63e−2	9.59e−1	1.16	2.71	6.39e−2	1.10e00	5.86	3.90
	41	3.30e−2	4.15e−1	1.29	3.23	2.77e−2	5.01e−1	9.80	5.77
	81	1.53e−2	1.93e−1	1.38	3.30	1.48e−2	2.44e−1	11.4	10.1
	161	7.36e−2	9.30e−2	1.42	3.23	8.08e−3	1.23e−1	10.9	19.8
0.1	21	4.63e−2	6.00e−1	1.71	1.74	5.31e−2	7.61e−1	7.65	1.79
	41	2.05e−2	2.49e−1	1.96	1.69	2.21e−2	3.56e−1	13.7	2.05
	81	9.76e−3	1.08e−1	2.14	1.61	1.05e−2	1.61e−1	14.5	2.83
	161	4.74e−3	5.16e−2	2.26	1.51	5.19e−3	7.61e−2	13.8	4.15
		$\|e_1\|$	$\|e_1\|_\infty$	C_{iso}	C_{ep}	$\|e_1\|$	$\|e_1\|_\infty$	C_{iso}	C_{ep}
$(k,m) = (0,1)$: *Piecewise linear interpolation*									
0.5	21	5.88e−2	4.63e−1	1.04	1.74	3.90e−2	3.63e−1	1.38	2.30
	41	1.08e−2	1.16e−1	1.19	2.40	8.74e−3	1.04e−1	1.42	2.85
	81	2.22e−3	2.13e−2	1.26	2.66	1.86e−3	2.53e−2	1.73	3.36
	161	5.05e−4	4.49e−3	1.28	2.51	3.74e−4	1.13e−2	1.63	3.52
0.1	21	3.21e−2	3.93e−1	1.39	1.41	2.49e−2	2.46e−1	1.74	1.43
	41	5.21e−3	5.83e−2	1.75	1.66	4.58e−3	3.90e−2	2.58	1.44
	81	1.18e−3	9.40e−3	1.82	1.46	1.08e−3	9.34e−3	2.28	1.35
	161	2.90e−4	2.80e−3	1.91	1.34	2.66e−4	2.85e−3	2.69	1.29
		$\|\nabla e_1\|$	$\|e_1\|_\infty$	C_{iso}	C_{ep}	$\|\nabla e_1\|$	$\|e_1\|_\infty$	C_{iso}	C_{ep}
$(k,m) = (1,1)$: *Piecewise linear interpolation*									
0.5	21	5.06	4.52e−1	1.06	2.02	5.55	4.41e−1	1.23	2.58
	41	2.16	1.14e−1	1.25	2.89	2.00	9.95e−2	1.41	2.88
	81	0.96	2.26e−2	1.35	3.36	0.78	2.54e−2	1.47	3.06
	161	0.45	4.20e−3	1.36	2.87	0.35	4.36e−3	1.44	2.81
0.1	21	3.37	3.08e−1	1.74	1.65	3.18	2.69e−1	1.55	1.51
	41	1.38	6.42e−2	2.24	2.24	1.32	4.00e−2	1.82	1.49
	81	0.67	1.49e−2	2.10	1.82	0.63	1.10e−2	2.05	1.36
	161	0.33	4.48e−3	2.12	1.49	0.31	2.69e−3	2.39	1.26

$$\operatorname{tr}\left(I+\frac{1}{\alpha}\nabla v\nabla v^{\mathrm{T}}\right)=\left(2+\frac{1}{\alpha}|\nabla v|^2\right)\gg 2\left(1+\frac{1}{\alpha}|\nabla v|^2\right)^{\frac{1}{2}}=2\left(\det\left(I+\frac{1}{\alpha}\nabla v\nabla v^{\mathrm{T}}\right)\right)^{\frac{1}{2}}.$$

This indicates that G is highly anisotropic. As a result, both conditions (41) and (42) are difficult to be satisfied by a mesh with small constants C_{iso} and C_{ep}. To reduce the anisotropic feature of G, we can use a larger α. For instance, we take

$$\alpha=\left[\frac{1}{|\Omega|}\int_\Omega|\nabla v|\,\mathrm{d}\boldsymbol{x}\right]^2, \tag{81}$$

the intensity parameter (53) defined for the Winslow-type monitor function ($k = m = 0$ and $n = 2$). The new results are listed in Table 5. It can be seen that both C_{iso} and C_{ep} have now much smaller values. For comparison purpose, we plot in Fig. 3 converged meshes obtained with α defined in (60) and (81).

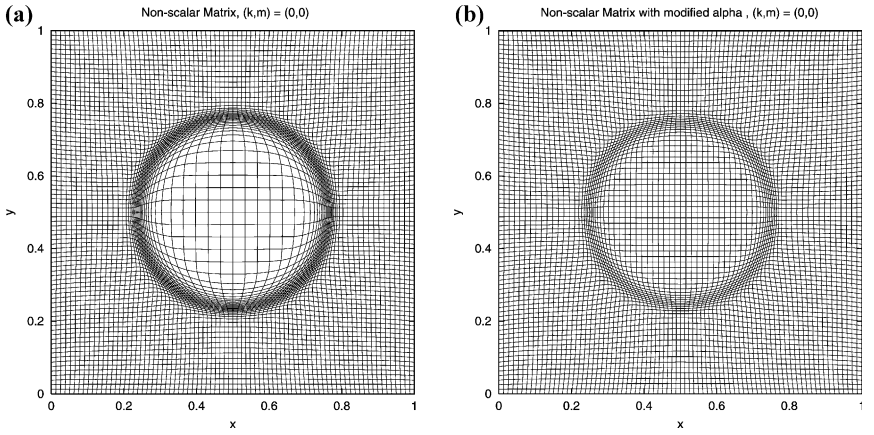

Fig. 3. Converged adaptive meshes for Example 1 are obtained using the variational method ($\theta = 0.1$) with the non-scalar matrix monitor function (58) based on function gradient. The difference in adaptive meshes is shown for different definitions of α; (a) with (60) and (b) with (81).

Table 4
Interpolation error is obtained on uniform meshes for Example 1

$J_{\max}$	Piecewise constant interpolation		Piecewise linear interpolation		
	$\|e_0\|$	$\|e_0\|_\infty$	$\|e_1\|$	$\nabla\|e_1\|$	$\|e_1\|_\infty$
21	1.21e − 1	1.46e00	8.143 − 2	6.11	5.08e − 1
41	6.39e − 2	8.58e − 1	2.48e − 2	3.60	2.45e − 1
81	3.23e − 2	4.58e − 1	6.60e − 3	1.89	7.32e − 2
161	1.62e − 2	2.32e − 1	1.69e − 3	0.96	1.92e − 2

It is interesting to note that scalar and non-scalar matrix monitor functions lead to very comparable results for this example, although generally speaking, the latter produces slightly greater C_{iso} and C_{ep}. Like in [16], the smaller θ is, the larger C_{iso} and the smaller C_{ep}.

Numerical results obtained on uniform meshes are listed in Table 4. For comparison purpose, the results for the maximum error are also listed. We can see that an adaptive mesh leads to more accurate results than a uniform mesh with the same number of points. The difference is significant, especially in the maximum error.

Table 5
Interpolation error for Example 1 on adaptive meshes obtained using the variational method ($\theta = 0.1$ or 0.5) with larger α (81) and a non-scalar matrix monitor function for piecewise constant interpolation

θ	$J_{\max}$	$\|e_0\|$	$\|e_0\|_\infty$	C_{iso}	C_{ep}
0.5	21	6.67e − 2	9.90e − 1	1.90	2.08
	41	2.77e − 2	3.99e − 1	1.99	2.70
	81	1.30e − 2	1.74e − 1	1.72	3.94
	161	6.22e − 3	8.05e − 2	1.51	5.34
0.1	21	7.08e − 2	9.12e − 1	2.57	1.36
	41	2.99e − 2	3.81e − 1	2.93	1.31
	81	1.38e − 2	1.72e − 1	2.93	1.31
	161	6.63e − 3	8.15e − 2	2.88	1.30

Finally, we note that in two dimensions, traditional monitor functions are different from the optimal monitor functions only for two cases with non-scalar matrix monitor functions, $(k,m)=(0,0)$ and $(k,m)=(1,0)$. The numerical results obtained for these cases with both traditional and optimal G are listed in Table 6. One can see that the traditional G defined in (63) leads to slightly better results than those with the optimal G (58). It is emphasized again that, as discussed in Section 4.1.1, an optimal monitor function does not necessarily produce the smallest error because the constant C in the error bound depends on the values of several other constants, including C_{iso} and C_{ep} that measure how close conditions (41) and (42) are satisfied.

Example 2. The second example is to generate adaptive meshes for a given analytical solution

$$\begin{aligned} v(x,y) = {} & \tanh\left(30\left(x^2+y^2-\frac{1}{8}\right)\right)+\tanh\left(30\left((x-0.5)^2+(x-0.5)^2-\frac{1}{8}\right)\right) \\ & +\tanh\left(30\left((x-0.5)^2+(x+0.5)^2-\frac{1}{8}\right)\right)+\tanh\left(30\left((x+0.5)^2+(x-0.5)^2-\frac{1}{8}\right)\right) \\ & +\tanh\left(30\left((x+0.5)^2+(x+0.5)^2-\frac{1}{8}\right)\right) \end{aligned} \tag{82}$$

defined in $[-2,2]\times[-2,2]$. This example is more difficult than Example 1 since the mesh points have to be concentrated to a more complicated region – the union of five circles.

Typical adaptive meshes obtained with scalar and non-scalar matrix monitor functions are plotted in Fig. 4. Once again, there is no significant difference between the results obtained with scalar and non-scalar matrix G, except for the case of piecewise constant interpolation with a non-scalar matrix G. For this case, the mesh lines are not aligned with tangential directions at the intersection of any two circles, such as $(x,y)=(-0.25,-0.25)$. In the neighborhood of this point, we have

$$v_x \approx 60(2x+0.5)\approx 0, \quad v_y \approx 60(2y+0.5)\approx 0$$

and

$$G = I + 1(1/\alpha)\nabla v(\nabla v)^{\mathrm{T}} \approx I.$$

Table 6
Comparison of traditional and optimal non-scalar monitor functions for the cases $(k,m)=0$ and $(k,m)=(1,0)$

$J_{\max}$	Traditional G (63) for G, (81) for α				Optimal G (58) for G, (60) for α			
	$\|e_0\|$	$\|e_0\|_\infty$	C_{iso}	C_{ep}	$\|e_0\|$	$\|e_0\|_\infty$	C_{iso}	C_{ep}
$(k,m)=(0,0)$								
21	4.39e−2	5.92e−1	2.18	1.64	5.31e−2	7.61e−1	7.65	1.79
41	1.91e−2	2.36e−1	2.20	1.44	2.21e−2	3.56e−1	13.7	2.05
81	8.90e−3	9.57e−2	2.23	1.36	1.05e−2	1.61e−1	14.5	2.83
161	4.48e−3	4.72e−2	2.23	1.39	5.19e−3	7.61e−2	13.8	4.15
	(73) for G, (70) for α				(67) for G, (70) for α			
	$\|e_1\|$	$\|e_1\|_\infty$	C_{iso}	C_{ep}	$\|e_1\|$	$\|e_1\|_\infty$	C_{iso}	C_{ep}
$(k,m)=(1,0)$								
21	1.84e−2	1.79e−1	2.07	1.78	2.49e−2	2.46e−1	1.74	1.43
41	3.90e−3	3.92e−2	2.48	1.62	4.58e−3	3.90e−2	2.58	1.44
81	1.18e−3	1.22e−2	3.53	1.88	1.083−3	9.34e−3	2.28	1.35
161	3.86e−4	3.98e−3	5.84	2.67	2.66e−4	2.85e−3	2.69	1.29

Interpolation error is shown for Example 1 on adaptive meshes obtained using the variational method ($\theta=0.1$).

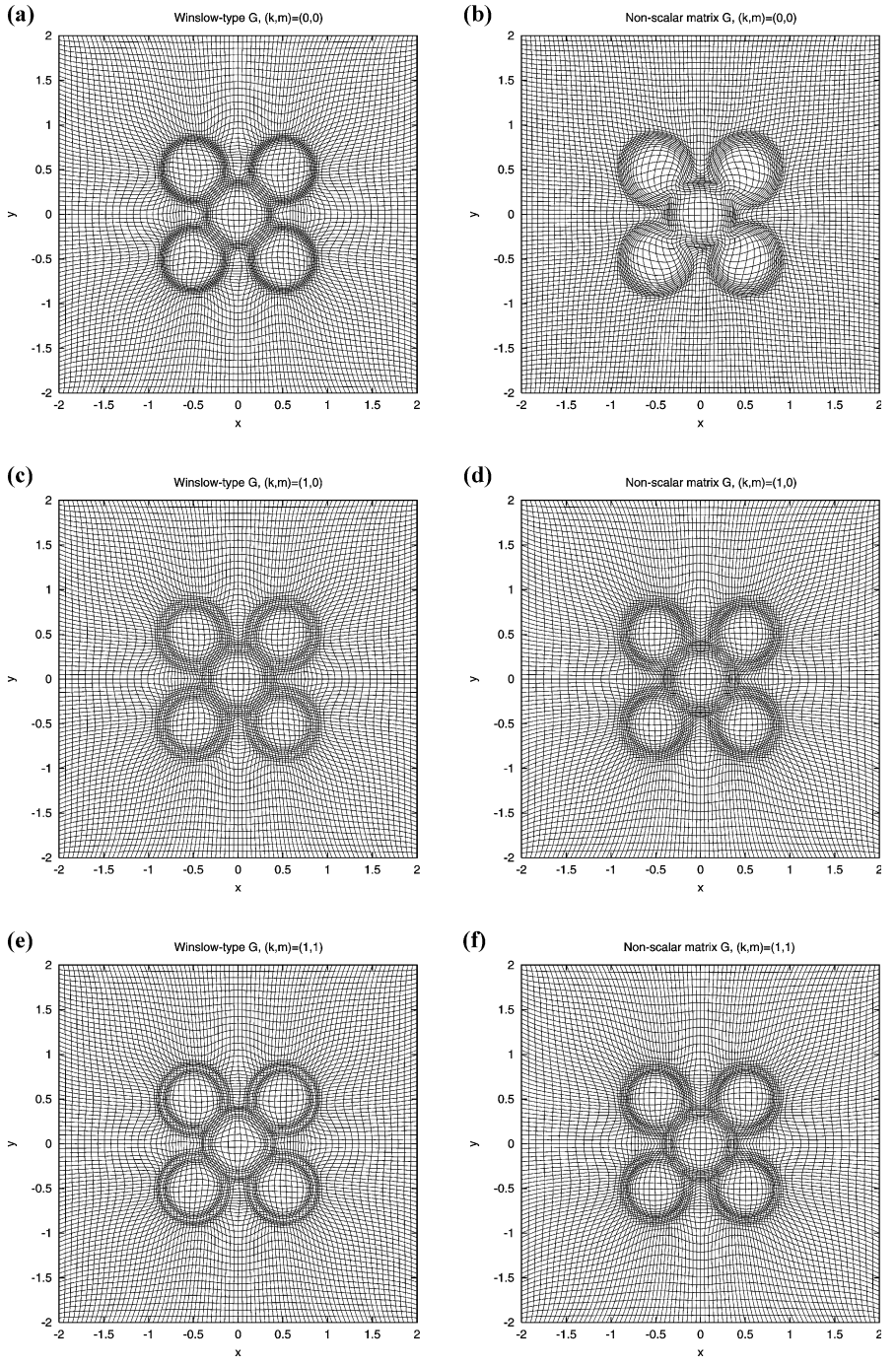

Fig. 4. Converged adaptive meshes of size 81×81 for Example 2 are obtained using the variational method ($\theta = 0.1$) with optimal monitor functions defined for piecewise constant interpolation $(k,m) = (0,0)$ and piecewise linear interpolation $(k,m) = (1,0)$ and $(1,1)$. The left column corresponds to Winslow-type monitor functions while the right column corresponds to non-scalar matrix ones. Rows 1, 2, and 3 correspond to the cases $(k,m) = (0,0),\ (1,0),$ and $(1,1)$, respectively.

Thus, the mesh tends to be rectangular around this point.

The other results are listed in Table 7. The corresponding results obtained with uniform meshes are listed in Table 8. They confirm the observations made for Example 1.

Example 3. The last example is the numerical solution of the boundary value problem of a convection dominated elliptic equation

$$R\frac{\partial u}{\partial x} = \frac{\partial^2 u}{\partial x^2} + \frac{\partial^2 u}{\partial y^2} + \omega^2\left(1 - e^{R(x-1)}\right)\sin(\omega y) \quad 0 < x, y < 1 \tag{83}$$

subject to Dirichlet boundary conditions that are chosen such that the exact solution is given

$$u(x, y) = \left(1 - e^{R(x-1)}\right)\sin(\omega y).$$

R and ω are taken as $R = 35$ and $\omega = 1.5\pi$. This example has been used by several researchers, e.g. [11], to demonstrate the efficiency of adaptive mesh methods.

Table 7
Interpolation error on adaptive meshes obtained for Example 2 ($R = 30$) using the variational method ($\theta = 0.1$) with optimal scalar and non-scalar matrix monitor functions for $(k, m) = (0, 0)$, (1,0), and (1,1)

$J_{\max}$	Winslow-type G				Non-scalar matrix G			
	$\|e_0\|$	$\|e_0\|_\infty$	C_{iso}	C_{ep}	$\|e_0\|$	$\|e_0\|_\infty$	C_{iso}	C_{ep}
$(k, m) = (0, 0)$: *Piecewise constant interpolation*								
21	4.23e − 1	1.52e00	1.36	1.83	4.99e − 1	1.69e00	9.03	2.34
41	1.61e − 1	9.30e − 1	2.13	1.81	2.12e − 1	1.03e00	20.3	2.71
81	7.41e − 2	4.77e − 1	2.92	1.66	9.18e − 2	7.88e − 1	57.5	4.29
161	3.58e − 2	2.12e − 1	3.98	1.55	4.51e − 2	2.64e − 1	48.7	5.77
	$\|e_1\|$	$\|e_1\|_\infty$	C_{iso}	C_{ep}	$\|e_1\|$	$\|e_1\|_\infty$	C_{iso}	C_{ep}
$(k, m) = (1, 0)$: *Piecewise linear interpolation*								
21	4.27e − 1	8.66e − 1	1.20	1.25	4.21e − 1	8.63e − 1	2.35	1.41
41	8.31e − 2	2.58e − 1	1.46	1.49	7.29e − 2	2.74e − 1	2.21	1.71
81	1.77e − 2	1.22e − 1	2.06	1.66	1.49e − 2	6.33e − 2	3.13	1.57
161	4.32e − 3	3.13e − 2	2.40	1.46	3.46e − 3	1.20e − 2	3.69	1.56
	$\|\nabla e_1\|$	$\|e_1\|_\infty$	C_{iso}	C_{ep}	$\|\nabla e_1\|$	$\|e_1\|_\infty$	C_{iso}	C_{ep}
$(k, m) = (1, 1)$: *Piecewise linear interpolation*								
21	11.1	7.98e − 1	1.33	1.40	11.5	7.17e − 1	1.82	1.42
41	5.30	3.20e − 1	1.64	1.91	4.75	2.89e − 1	2.29	1.85
81	3.04	2.06e − 1	2.61	2.26	2.24	1.02e − 1	4.28	1.77
161	1.62	5.63e − 2	3.20	1.69	1.07	1.64e − 2	3.92	2.52

Table 8
Interpolation error is obtained on uniform meshes for Example 2 ($R = 30$)

$J_{\max}$	Piecewise constant interpolation		Piecewise linear interpolation		
	$\|e_0\|$	$\|e_0\|_\infty$	$\|e_1\|$	$\|\nabla e_1\|$	$\|e_1\|_\infty$
21	7.08e − 1	1.79e00	5.82e − 1	12.6	9.04e − 1
41	4.04e − 1	1.31e00	1.91e − 1	7.83	7.31e − 1
81	1.99e − 1	7.53e − 1	7.06e − 2	5.09	3.08e − 1
161	1.00e − 1	3.91e − 1	1.85e − 2	2.64	9.12e − 2

The differential equation is first transformed into the computational domain and discretized on a uniform computational mesh using central finite differences. The resultant system consisting of the physical and mesh equations is solved alternately for the physical solution and the adaptive mesh. The convergent results are obtained when the difference in the physical solution at two consecutive iterates is small. For this problem, the physical solution has a sharp boundary layer at $x = 1$. Since a uniform distribution of boundary points cannot lead to accurate solutions, we use a non-uniform one that is generated using the one-dimensional mesh equation (i.e. the Euler–Lagrange equation of the 1D version of $I[\xi]$), see e.g. [15] for detail. e_0 and e_1 denote the error functions for the piecewise constant and linear interpolation of the computed solution, respectively. (The interpolation polynomials are computed in the same manner as in the previous two examples but with the nodal function values being replaced by the computed solution values.)

Table 9
(Example 3) Solution error on adaptive meshes obtained with the variational method ($\theta = 0.1$) using scalar and non-scalar matrix monitor functions

$J_{\max}$	Winslow-type G		Non-scalar matrix G	
	$\|e_0\|$ (ratio)	$\|e_0\|_\infty$ (ratio)	$\|e_0\|$ (ratio)	$\|e_0\|_\infty$ (ratio)
G is calculated with $(k,m) = (0,0)$				
17	5.53e − 2	4.83e − 1	5.53e − 2	3.69e − 1
33	2.63e − 2 (2.1)	2.43e − 1 (2.0)	2.70e − 2 (2.0)	1.88e − 1 (2.0)
65	1.30e − 2 (2.0)	1.21e − 1 (2.0)	1.34e − 2 (2.0)	9.61e − 2 (2.0)
129	6.47e − 3 (2.0)	6.11e − 2 (2.0)	6.73e − 3 (2.0)	4.79e − 2 (2.0)
	$\|e_1\|$ (ratio)	$\|e_1\|_\infty$ (ratio)	$\|e_1\|$ (ratio)	$\|e_1\|_\infty$ (ratio)
G is calculated with $(k,m) = (1,0)$				
17	1.01e − 2	1.62e − 1	9.66e − 3	1.10e − 1
33	1.89e − 3 (5.3)	4.84e − 2 (3.3)	1.71e − 3 (5.6)	2.83e − 2 (3.9)
65	4.21e − 4 (4.5)	1.31e − 2 (3.7)	3.68e − 4 (4.6)	7.32e − 3 (3.9)
129	1.02e − 4 (4.1)	3.74e − 3 (3.5)	1.05e − 4 (3.5)	2.88e − 3 (2.5)
	$\|\nabla e_1\|$ (ratio)	$\|e_1\|_\infty$ (ratio)	$\|\nabla e_1\|$ (ratio)	$\|e_1\|_\infty$ (ratio)
G is calculated with $(k,m) = (1,1)$				
17	8.68e − 1	1.34e − 1	1.00e00	9.86e − 2
33	3.90e − 1 (2.2)	3.81e − 2 (3.5)	3.86e − 1 (2.6)	2.54e − 2 (3.9)
65	1.85e − 1 (2.1)	9.82e − 3 (3.9)	1.63e − 1 (2.4)	5.77e − 3 (4.4)
129	9.43e − 2 (2.0)	2.81e − 3 (3.5)	7.69e − 2 (2.1)	1.38e − 3 (4.2)

e_0 and e_1 denote the error functions for the piecewise constant and piecewise linear interpolation of the computed solution, respectively. (That is, the interpolation polynomials are computed based on the nodal values of the computed solution.)

Table 10
(Example 3) Solution error on uniform meshes, e_0 and e_1 denote the error functions for the piecewise constant and piecewise linear interpolation of the computed solution, respectively. (That is, the interpolation polynomials are computed based on the nodal values of the computed solution.)

$J_{\max}$	Piecewise constant interpolation		Piecewise linear interpolation		
	$\|e_0\|$ (ratio)	$\|e_0\|_\infty$ (ratio)	$\|e_1\|$ (ratio)	$\|\nabla e_1\|$ (ratio)	$\|e_1\|_\infty$ (ratio)
17	6.81e − 2	6.86e − 1	2.52e − 2	1.78e00	2.28e − 1
33	3.47e − 2 (2.0)	4.70e − 1 (1.5)	6.85e − 3 (3.7)	9.66e − 1 (1.8)	8.94e − 2 (2.6)
65	1.75e − 2 (2.0)	2.86e − 1 (1.6)	1.75e − 3 (3.9)	4.94e − 1 (2.0)	2.86e − 2 (3.1)
129	8.74e − 3 (2.0)	1.60e − 1 (1.8)	4.39e − 4 (4.0)	2.49e − 1 (2.0)	8.16e − 3 (3.5)

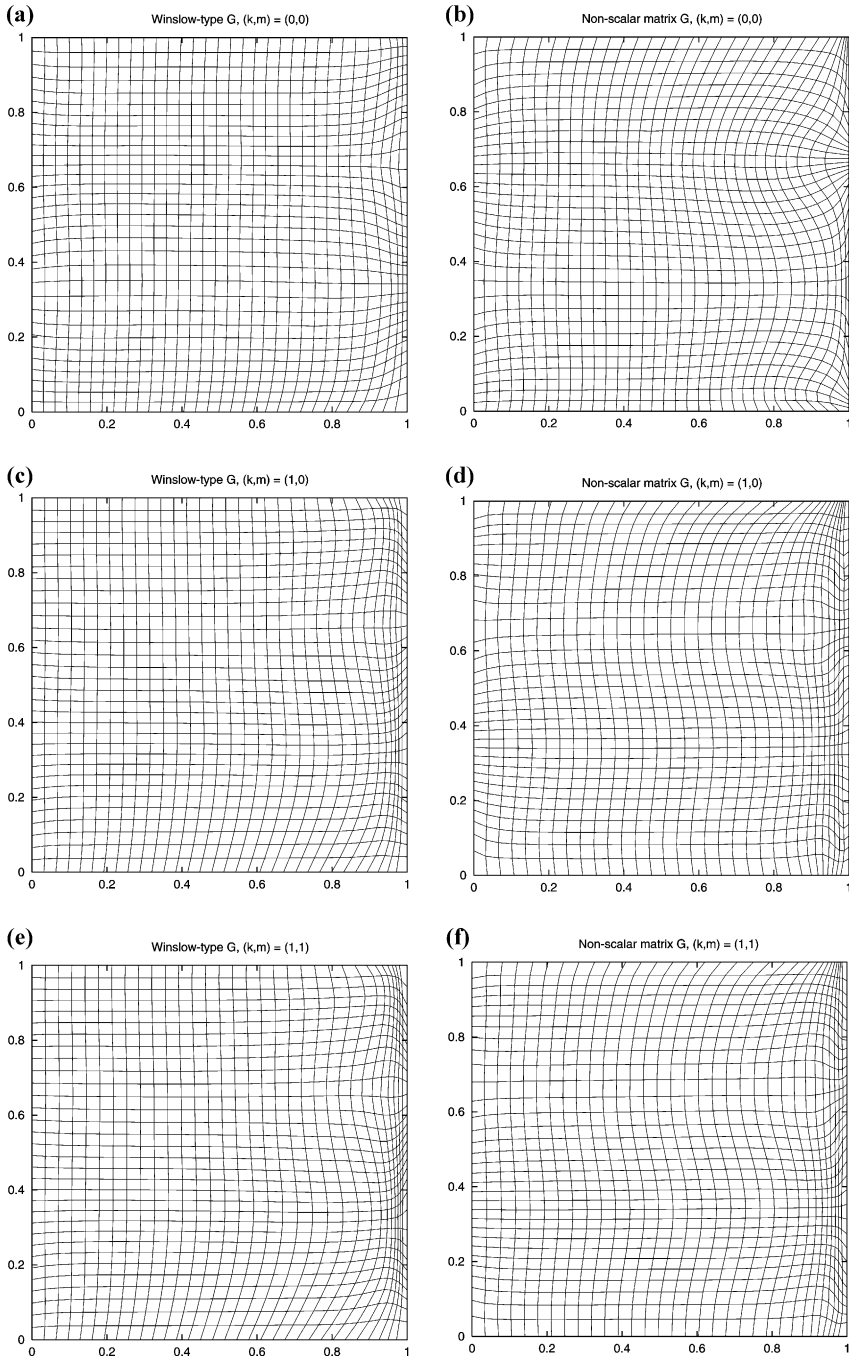

Fig. 5. Converged adaptive meshes of size 33×33 for Example 3 are obtained using the variational method ($\theta = 0.1$) with optimal monitor functions defined for piecewise constant interpolation $(k, m) = (0, 0)$ and piecewise linear interpolation $(k, m) = (1, 0)$ and $(1, 1)$. The left column corresponds to Winslow-type monitor functions while the right column corresponds to non-scalar matrix ones. Rows 1, 2, and 3 correspond to the cases $(k, m) = (0, 0),\ (1, 0),$ and $(1, 1)$, respectively.

Note that both $\|e_0\|_\infty$ and $\|e_1\|_\infty$ are different from (and in fact greater than) the nodal maximum error of the solution.

The numerical results obtained on adaptive and uniform meshes are listed in Tables 9 and 10, respectively. Overall, the non-scalar matrix monitor functions lead to slightly better results than those of Winslow's type. Once again, the results confirm the theoretical prediction on convergence, namely, $\|e_0\| = O(h_c)$, $\|e_1\| = O(h_c^2)$, and $\|\nabla e_1\| = O(h_c)$, where $h_c = 1/G\boldsymbol{J}_{\max} = 1/K_{\max}$. Finally, typical adaptive meshes are shown in Fig. 5.

6. Conclusions

In the previous sections we have developed several (asymptotic) interpolation error estimates in terms of a general coordinate transformation between the physical and computational domains. Both scalar (Window's type) and non-scalar matrix monitor functions are defined based on these estimates for the variational mesh adaptation method developed in [16]. These monitor functions are optimal in the sense that they lead to the smallest physical-solution-dependent factor in error bounds. The choice of the intensity parameter is also given for each monitor function.

The regularity and equidistribution conditions (41) (or (69)) and (42) play a crucial role in the development. They formulate the approximate satisfaction of the isotropic and equidistribution criteria used in [16] for designing the mesh adaptation functional. They can be used as measures for mesh regularity and adaptation. Indeed, a mesh that satisfies (41) with a Window-type monitor function and $C_{\text{iso}} = 1$ will consist of only equilateral cells. For a non-scalar matrix monitor, the mesh regularity can be better understood in a Riemannian space having the monitor function as its metric tensor. An isotropic mesh in this space can have skewed cells in the physical domain.

Under the regularity and equidistribution conditions we have obtained asymptotic interpolation error bounds on adaptive meshes. It is shown that these bounds are generally much smaller than those obtained on a uniform mesh for rough functions. Similar interpolation error bounds are also obtained for several traditional monitor functions. Most of them are not optimal. However, the difference in the interpolation error on adaptive meshes obtained with optimal and non-optimal monitor functions are not as great as that on adaptive meshes and uniform meshes. This observation, together with continuous dependence of error bounds on C_{iso} and C_{ep} (see (41) and (42)), indicates that the optimal error bounds are rather stable to perturbations of the optimal meshes. This is consistent with the observations made by Babuska and Rheinboldt [1] and de Boor [10] for one-dimensional problems. Moreover, a non-optimal monitor function can lead to reasonably accurate results as long as it stays to some extent close to the optimal one. This may explain why many existing methods can have a certain degree of success even though they do not produce an optimal adaptive mesh.

We have presented two-dimensional numerical results obtained using the method of [16] with the monitor functions developed in Section 4 for three examples. The results show that the method is able to produce adaptive meshes that satisfy the regularity and equidistribution conditions. The theoretical prediction on convergence orders are verified by the numerical results.

References

[1] I. Babuska, W.C. Rheinboldt, A posteriori error estimates for the finite element method, Int. J. Numer. Meth. Eng. 12 (1978) 1597–1615.

[2] M.J. Baines, S.J. Leary, Fluctuations and signals for scalar hyperbolic equations on adjustable meshes, Comm. Numer. Meth. Eng. 15 (1999) 877–886.

[3] R.E. Bank, R.K. Smith, Mesh smoothing using a posteriori error estimates, SIAM J. Numer. Anal. 34 (1997) 979–997.

[4] G. Beckett, J.A. Mackenzie, Convergence analysis of finite-difference approximations on equidistributed grids to a singularly perturbed boundary value problems, J. Comput. Appl. Math. 35 (2000) 109–131.
[5] J.U. Brackbill, An adaptive grid with directional control, J. Comput. Phys. 108 (1993) 35–50.
[6] J.U. Brackbill, J.S. Saltzman, Adaptive zoning for singular problems in two dimensions, J. Comput. Phys. 46 (1982) 342–368.
[7] G.F. Carey, H.T. Dinh, Grading functions and mesh redistribution, SIAM J. Numer. Anal. 22 (1985) 1028–1040.
[8] K. Chen, Error equidistribution and mesh adaptation, SIAM J. Sci. Comput. 15 (1994) 798–818.
[9] P.G. Ciarlet, The Finite Element Method for Elliptic Problems, North-Holland, Amsterdam, 1978.
[10] C. de Boor, Good approximation by splines with variables knots ii, in: G.A. Watson (Ed.), Lecture Notes in Mathematics vol. 363, Springer, Berlin, 1974, pp. 12–20 (Conference on the Numerical Solution of Differential Equations, Dundee, Scotland, 1973).
[11] A.S. Dvinsky, Adaptive grid generation from harmonic maps on Riemannian manifolds, J. Comput. Phys. 95 (1991) 450–476.
[12] J.E. Castillo (Ed.), Mathematics Aspects of Numerical Grid Generation, SIAM, Philadelphia, 1991.
[13] L.C. Evans, Partial Differential Equations, Graduate Studies in Mathematics, vol. 19, American Mathematical Society, Providence, RI, 1998.
[14] R. Hagmeeijer, Grid adaption based on modified anisotropic diffusion equations formulated in the parametric domain, J. Comput. Phys. 115 (1994) 169–183.
[15] W. Huang, Practical aspects of formulation and solution of moving mesh partial differential equations, J. Comput. Phys. 171 (2001) 753–775.
[16] W. Huang, Variational mesh adaptation: isotropy and equidistribution, J. Comput. Phys. 174 (2001) 903–924.
[17] P.M. Knupp, Mesh generation using vector-fields, J. Comput. Phys. 119 (1995) 142–148.
[18] P.M. Knupp, S. Steinberg, Fundamentals of Grid Generation, CRC Press, Boca Raton, 1994.
[19] P.M. Knupp, Jacobian-weighted elliptic grid generation, SIAM J. Sci. Comput. 17 (1996) 1475–1490.
[20] P.M. Knupp, N. Robidoux, A framework for variational grid generation: conditioning the Jacobian matrix with matrix norms, SIAM J. Sci. Comput. 21 (2000) 2029–2047.
[21] H. Kober, On the arithmetic and geometric means and on hölder's inequality, Proc. Am. Math. Soc. 9 (1958) 452–459.
[22] V.D. Liseikin, Grid Generation Methods, Springer, Berlin, 1999.
[23] Yu.G. Reshetnyak, in: Space Mappings with Bounded Distortion, Translation of Mathematical Monographs, vol. 73, American Mathematical Society, Providence, RI, 1989.
[24] R. Schoen, S.T. Yau, On univalent harmonic maps between surfaces, Inv. Math. 44 (1978) 265–278.
[25] S. Steinberg, P.J. Roache, Variational grid generation, Numer. Meth. P.D.E. 2 (1986) 71–96.
[26] J.F. Thompson, Z.A. Warsi, C.W. Mastin, Numerical Grid Generation: Foundations and Applications, North-Holland, New York, 1985.
[27] Y. Tourigny, M.J. Baines, Analysis of an algorithm for generating locally optimal meshes for L_2 approximation by discontinuous piecewise polynomials, Math. Comp. 66 (1997) 623–650.
[28] Y. Tourigny, F. Hülsemann, A new moving mesh algorithm for the finite element solution of variational problems, SIAM J. Numer. Anal. 35 (1998) 1416–1438 (electronic).
[29] A. Winslow, Numerical solution of the quasi-linear Poisson equation in a nonuniform triangle mesh, J. Comput. Phys. 1 (1967) 149–172.